Università degli Studi di Padova
Dipartimento di Fisica e Astronomia "Galileo Galilei"
Dipartimento di Ingegneria dell'Informazione

Corso di Laurea Magistrale in Fisica

Entangled States on one or more degrees of freedom and their application to Fundamental Physics

RELATORE: Chiar.mo Prof. Paolo Villoresi
CONTRORELATORE: Chiar.mo Prof. Michele Merano,
CORRELATORE: Chiar.mo Prof. Giuseppe Vallone,
Dott. Marco Tomasin

LAUREANDO: Elia Mantoan

Anno Accademico 2014/2015

Contents

Abstract

Quantum Mechanics is one of the fundamental branch of physics which deals with the world at the nanoscale ($\lesssim 10^{-9}\, m$) where we found the quantum particles. When experiments could not be explained by Classical Mechanics, Quantum Mechanics was born and at the beginning it was just a set of controversial mathematical explanations. One of the interesting aspect is the quantum entanglement, which is a physical phenomenon where two or more particles are generated or interact in such way that a measure performed in a part of the system will instantaneously influence the results of the measure on the remaining part. This means that the particles can not be described separately and the system has a non local behavior and so the quantum state may be given for the system as a whole. During the '80 some scientists understood that this particular behavior of quantum particles can be exploited to use in communication and computation fields. For example Richard Feynman in 1982 showed that a classical Turing machine is exponentially slower when it's used to simulate quantum phenomena than his hypothetical quantum version. Quantum computation, quantum cryptography, quantum dense coding, quantum entanglement, quantum teleportation get great advantage compared with the correspondent classical protocol.

The goal of our experiment is first to demonstrate that a local realist model with long realist delays can not describe the physical results and second to successfully perform an hyperentangled[1] communication in free space using photons as a means. In this experiment photons, entangled in polarization and time-bin, are used. We achieve to prove that these states engrave the characteristic of hyperentagled quantum states and that they can not describe a local realist model. In order to show this, techniques such as quantum tomography and Chained Bell's measurements are used .

[1] Particle entangled in more than one degrees of freedom.

Chapter 1

Quantum information

In this chapter we introduce how the entanglement was born, the Bell's inequality that is a measure which, using an entangled state, it allows to discriminate if a local hidden variable theory can describe the physical world and the Density Matrix that allows to express a quantum state. After this, we introduce a set of quantum protocols that work using entangled or hyperentangled states like the quantum key distribution, the quantum dense coding and the quantum teleportation.

1.1 EPR Paradox

Last century saw the birth of some of the greatest scientific revolution. One of the most important revolution is sure the quantum mechanic. In the 1935 the theoretical understanding of the quantum theory was based on the Bohr's ideas. According to Bohr view, when a measure is performed on a quantum object, this involves a physical interaction with the measuring device that affects both systems. This interaction is what performs the measurement "result" and, because it is uncontrollable, that can only be predicted statistically. So if the position of particle is observed, than its momentum is uncontrollably affected[1]. Einstein was firstly enthusiastic about the quantum theory but he had some reservation that led him in May 15, 1935 to publish "Can Quantum-Mechanics Description of Physical Reality Be Considered Complete?".

1.1.1 The argument of EPR Paradox

In the article Einstein, Podolsky and Rosen affirmed that the physical description of quantum mechanics can not be complete. First they gave the following definition:

Complete theory: A theory is complete if every element of the physical reality has a counter part in the physical theory.

[1] Heisenberg's Uncertainty Principle

Reality: A sufficient condition for the reality of a physical quantity is the possibility of predicting it with certainty, without disturbing the system.

Locality: An action execute on a system A can not affect a system B time-separated.

A theory can be considered satisfactory, they affirmed, only if it is correct and its description is complete. The correctness of a theory is assessed by the prevision of a theory and what human being experiences. The quantum mechanics surely fulfill these points. About the completeness they said that: "Quantum Mechanics is **not complete** or two **non-commuting observables cannot have simultaneous reality**".

Let's consider the following system (spin state):

$$|\psi\rangle = \frac{1}{\sqrt{2}} \left(|\uparrow\rangle_A |\downarrow\rangle_B - |\downarrow\rangle_A |\uparrow\rangle_B \right) \tag{1.1}$$

where A indicates Alice system, B indicates Bob system. If Alice executes a spin measure along z-axis and leaves $|\psi\rangle$in the state $|\uparrow\rangle_A |\downarrow\rangle_B$ than Bob can predict his states $|\downarrow\rangle_B$ and his eigenvalue along z-axis without disturbing his particle. Now let's think that Alice executes a measure on x-axis, in the same way as before Bob can predict his eigenvalue on x-axis. So, from the reality definition, we can affirm that both $\sigma_{x,\,bob}$ and $\sigma_{z,\,bob}$ are elements of reality. Anyway from quantum mechanic we know that

$$[\sigma_i, \sigma_j] = 2i\epsilon_{ijk}\sigma_k \tag{1.2}$$

and from Heisenberg's Uncertainty Principle we can affirm that

$$\left\langle (\Delta A)^2 (\Delta B)^2 \right\rangle \geq \frac{|[A,\, B]|^2}{4} \tag{1.3}$$

so if both $\sigma_{x,\,Bob}$and $\sigma_{z,\,Bob}$ have simultaneous realities, the perfect knowledge of $\sigma_{x,\,Bob}$ implies the perfect uncertainty of $\sigma_{z,\,Bob}$. This leads to say that the quantum mechanic can not describe all elements of reality and that "Quantum Mechanics is not complete or two non-commuting observables cannot have simultaneous reality".

1.2 Entanglement

This particular state of matter of a strongly correlated system was first treated in the EPR Paradox. However the one that first coined the word entanglement was Erwin Schrödinger that used it to describe the correlation between two particles that interact and then separate, as in the EPR experiment. In the paper "Discussion of probability relations between separated systems" he defined and discussed the notion and termed it "entanglement".

A definition of entangled system is: a quantum state cannot be factored as a product of states of its local constituent. Consider a two particles system with

states $|\psi\rangle$ and a single particle states $|\varphi\rangle_A$ and $|\omega\rangle_B$ which lie respectively in $\mathcal{H}_A$ and $\mathcal{H}_B$ Hilbert spaces. The system is entangled if the whole system $|\psi\rangle$ can not be separated in the product of single Hilbert spaces $\mathcal{H}_A$ and $\mathcal{H}_B$.

$$|\psi\rangle \neq |\varphi\rangle_A \otimes |\omega\rangle_B \tag{1.4}$$

1.3 Bell Inequality

About thirty years later, in 1964, John S. Bell wrote a paper regarding what later was called Bell's inequality. In the paper he explained a method to verify if a local hidden variable theory was correct or wrong, performing a set of measures using an entangled state. Regarding his demonstration, he used a pair of spin $\frac{1}{2}$ particles formed somehow in the singlet spin state, moving in opposite direction, inside a measurement apparatus that can perform measure in selected components of the spin σ_1 and σ_2. If a measurement is performed along the $\vec{a}$ direction, if $\vec{\sigma_1} \cdot \vec{a} = +1$ then, according to quantum mechanics, $\vec{\sigma_2} \cdot \vec{a} = -1$ independently by the distance of the two particles and the time of the measurement. This suggested that the value of measurement must be predetermined. However the wave-function does not determine the result of an individual measurement so this implies that a more complete representation of the wave function could exist. Let's think that this new representation is affected by a parameter λ[2]. In this system then the result A of a measurement $\vec{\sigma_1} \cdot \vec{a}$ is determined by $\vec{a}$ and λ and the result B of a measurement $\vec{\sigma_2} \cdot \vec{b}$ is determined by $\vec{b}$ and λ.

$$A(\vec{a}, \lambda) = \pm 1,\ B(\vec{b}, \lambda) = \pm 1 \tag{1.5}$$

Note that it is assumed that the result of B does not depend on the value of $\vec{a}$ and vice versa A on $\vec{b}$. With the above assumption and if $\rho(\lambda)$ represents the probability distribution of λ then the expectation value of the product of the two components A and B is

$$E(\vec{a}, \vec{b}) = \int d\lambda \rho(\lambda) A(\vec{a}, \lambda) B(\vec{b}, \lambda) \tag{1.6}$$

and it should be equal to the quantum mechanical expectation value which for the singlet states is

$$\left\langle \vec{\sigma_1} \cdot \vec{a}\, \vec{\sigma_2} \cdot \vec{b} \right\rangle = -\vec{a} \cdot \vec{b} \tag{1.7}$$

but this is not possible. To demonstrate this we use the CHSH inequality. We define

$$S(\vec{a}, \vec{b}, \vec{a'}, \vec{b'}) = E(\vec{a}, \vec{b}) - E(\vec{a}, \vec{b'}) + E(\vec{a'}, \vec{b}) + E(\vec{a'}, \vec{b'}) \tag{1.8}$$

where

$$E(\vec{a}, \vec{b}) = \frac{C(\vec{a}, \vec{b}) - C(\vec{a_\perp}, \vec{b}) - C(\vec{a}, \vec{b_\perp}) + C(\vec{a_\perp}, \vec{b_\perp})}{C(\vec{a}, \vec{b}) + C(\vec{a_\perp}, \vec{b}) + C(\vec{a}, \vec{b_\perp}) + C(\vec{a_\perp}, \vec{b_\perp})} \tag{1.9}$$

[2] a single or a set of (hidden) variables

and

$$C(\vec{a},\vec{b}) = \int d\lambda \rho(\lambda) \frac{1+A(\vec{a},\lambda)}{2} \frac{1+B(\vec{b},\lambda)}{2} \tag{1.10}$$

represent the coincidences that are revealed on the receiver that is when $A(\vec{a},\lambda) = 1$ $(+1)$.

LHV theories main idea is that the non local behavior found in the description of Quantum Mechanics derives from some hidden variables that relate the results of the measurements. Using formula number 4 with number 3 we obtain:

$$\begin{aligned}
\left|S(\vec{a},\vec{b},\vec{a'},\vec{b'})\right| &= \left|\int d\lambda\rho(\lambda)\left[A(\vec{a},\lambda)B(\vec{b},\lambda) - A(\vec{a},\lambda)B(\vec{b'},\lambda) + A(\vec{a'},\lambda)B(\vec{b},\lambda) + A(\vec{a'},\lambda)B(\vec{b'},\lambda)\right]\right| \\
&\leq \int d\lambda\rho(\lambda)\left|A(\vec{a},\lambda)\left(B(\vec{b},\lambda) - B(\vec{b'},\lambda)\right) + A(\vec{a'},\lambda)\left(B(\vec{b},\lambda) + B(\vec{b'},\lambda)\right)\right| \\
&\leq \int d\lambda\rho(\lambda) 2 = 2
\end{aligned} \tag{1.11}$$

and therefore we obtain

$$|S| \leq 2. \tag{1.12}$$

Using quantum mechanics the S parameter becomes

$$S(\vec{a},\vec{b},\vec{a'},\vec{b'}) = \left\langle \vec{\sigma_1}\cdot\vec{a}\,\vec{\sigma_2}\cdot\vec{b}\right\rangle - \left\langle \vec{\sigma_1}\cdot\vec{a}\,\vec{\sigma_2}\cdot\vec{b'}\right\rangle + \left\langle \vec{\sigma_1}\cdot\vec{a'}\,\vec{\sigma_2}\cdot\vec{b}\right\rangle + \left\langle \vec{\sigma_1}\cdot\vec{a'}\,\vec{\sigma_2}\cdot\vec{b'}\right\rangle \tag{1.13}$$

and by selecting four vectors that have an internal angle separation of $\frac{\pi}{4}$ the S assumes value $|S| = 2\sqrt{2}$ that violates the above inequality.

1.4 Density Matrix

The density matrix operator is a tool developed to represent a system with numerable possible levels in a more affordable way than the wavefunction. This characteristic makes it interesting to describe two particles entangled system. Even more, thanks to quantum tomography it can be used to compare the measured data with what theory predicts.

A density matrix is a matrix that describes a quantum system in a mixed state, a statistical ensemble of several quantum states.

Explicitly, suppose a quantum system may be found in state $|\psi_1\rangle$ with probability p_1, or it may be found in state $|\psi_2\rangle$ with probability p_2, or it may be found in state $|\psi_3\rangle$ with probability p_3, and so on. The density operator for this system is

$$\hat{\rho} = \sum_i p_i |\psi_i\rangle\langle\psi_i| \tag{1.14}$$

where $\{|\psi_i\rangle\}$ don't need to be orthogonal. If we introduce an orthogonal basis $\{|u_i\rangle\}$ we call density matrix the element

$$\rho_{mn} = \langle u_m|\,\hat{\rho}\,|u_n\rangle = \sum_i p_i \langle u_m|\psi_i\rangle\langle\psi_i|u_n\rangle \tag{1.15}$$

Practically the density matrix can also be defined as

$$\hat{\rho} = \sum_{m,n} |u_m\rangle \, \rho_{mn} \, \langle u_n| \, . \tag{1.16}$$

From this definition, since p_i represents a probability, it's possible to observe that

$$\begin{aligned} &\sum_i p_i = 1 \\ &0 \leq p_i \leq 1, \, \forall i \\ &\sum_i p_i^2 \leq 1 \end{aligned} \tag{1.17}$$

From these conditions we obtain that $\hat{\rho}$ will be positive semi-definite. By the third condition, $\sum_i p_i^2 \leq 1$, it is possible to distinguish two particular cases:

- If $\sum_i p_i^2 < 1$, then we have a Mixed State, in which p_i assume several values. This represents the most common case.
- If $\sum_i p_i^2 = 1$ then there's only one p_i that assumes value 1 and all the others are 0. Because of this characteristic, it's possible to write the density operator as

  $$\hat{\rho} = |\psi\rangle \, \langle\psi| \tag{1.18}$$

  where $|\psi\rangle$ is the state with unitary probability. This represents a pure state.

Let us see some property of the density operator: $tr\hat{\rho} = 1$. It can be easily demonstrated if you consider an orthogonal basis $\{|u_n\rangle\}$

$$\begin{aligned} tr\hat{\rho} &= \sum_n \sum_i \langle u_n|p_i|\psi_i\rangle\langle\psi_i|u_n\rangle \\ &= \sum_n \sum_i p_i \langle u_n|\psi_i\rangle\langle\psi_i|u_n\rangle \\ &= \sum_i \sum_n p_i \langle\psi_i|u_n\rangle\langle u_n|\psi_i\rangle \\ &= \sum_i p_i \langle\psi_i| \left(\sum_n |u_n\rangle\langle u_n| \right) |\psi_i\rangle \\ &= \sum_i p_i \langle\psi_i|\psi_i\rangle \\ &= \sum_i p_i = 1 \end{aligned} \tag{1.19}$$

where we have used the completeness relation. Since we have not put any condition on p_i values, this equation holds both for mixed and pure states, so

it can not be used to distinguish them. Now let us investigate the property of the square of matrix density. In case of pure state we can write that

$$\hat{\rho}^2 = (|\psi\rangle\langle\psi|)(|\psi\rangle\langle\psi|) = |\psi\rangle\langle\psi|\psi\rangle\langle\psi| = |\psi\rangle\langle\psi| = \hat{\rho} \tag{1.20}$$

consequently

$$tr\hat{\rho}^2 = tr\hat{\rho} = 1. \tag{1.21}$$

Instead when we work with mixed state we obtain

$$\begin{aligned} \hat{\rho}^2 &= \left(\sum_i p_i|\psi_i\rangle\langle\psi_i|\right)\left(\sum_j p_j|\psi_j\rangle\langle\psi_j|\right) \\ &= \sum_i\sum_j p_i p_j|\psi_i\rangle\langle\psi_i|\psi_j\rangle\langle\psi_j| \end{aligned} \tag{1.22}$$

by this formula we find that

$$\begin{aligned} tr\hat{\rho}^2 &= \sum_n\sum_i\sum_j\langle u_n|p_i p_j|\psi_i\rangle\langle\psi_i|\psi_j\rangle\langle\psi_j|u_n\rangle \\ &= \sum_n\sum_i\sum_j p_i p_j\langle u_n|\psi_i\rangle\langle\psi_i|\psi_j\rangle\langle\psi_j|u_n\rangle \\ &= \sum_i\sum_j p_i p_j\langle\psi_j|\sum_n(|u_n\rangle\langle u_n|)|\psi_i\rangle\langle\psi_i|\psi_j\rangle \\ &= \sum_i\sum_j p_i p_j\langle\psi_j|\psi_i\rangle\langle\psi_i|\psi_j\rangle \\ &= \sum_i\sum_j p_i p_j|\langle\psi_i|\psi_j\rangle|^2 \\ &\leq \left(\sum_i p_i\right)^2 \end{aligned} \tag{1.23}$$

The equality case can be reached only if there is only a unitary probability in the p_i ensemble (pure state) or if $|\langle\psi_i|\psi_j\rangle|^2 = 1$, $\forall i, j$ (always pure state). Thus we reach the conclusion that

$$\begin{aligned} tr\hat{\rho}^2 &= 1 pure\, state \\ tr\hat{\rho}^2 &< 1 mixed\, state \end{aligned} \tag{1.24}$$

This results helpful in order to check the purity of the measured state so we define

$$\mathcal{P} = tr\hat{\rho}^2 \tag{1.25}$$

The density matrix is also very useful to calculate the expected value of a measure. In fact if O is an observable with associated operator $\hat{O}$, the expectation

value $\langle O \rangle$ is given by

$$\begin{aligned}
\langle O \rangle &= \sum_i p_i \langle \psi_i | \hat{O} | \psi_i \rangle \\
&= \sum_i \sum_j p_i \langle \psi_i | \hat{O} | u_j \rangle \langle u_j | \psi_i \rangle \\
&= \sum_i \sum_j p_i \langle u_j | \psi_i \rangle \langle \psi_i | \hat{O} | u_j \rangle \\
&= \sum_j \langle u_j | \left(\sum_i p_i | \psi_i \rangle \langle \psi_i | \right) \hat{O} | u_j \rangle \\
&= \sum_j \langle u_j | \hat{\rho} \hat{O} | u_j \rangle \\
&= tr \left(\hat{\rho} \hat{O} \right)
\end{aligned} \tag{1.26}$$

1.5 Quantum cryptography

Born by the need to maintain secret a communication, cryptography is a technique that secures a communication channel between two or more people over an insecure communication channel. Suppose two users, Alice and Bob that wish to secretly exchange information over a long distance, uncompromised by the possible presence of a third party-eavesdropper Eve located somewhere along the communication channel. The present strategy for doing this is to employ the public key cryptosystem, the most widely used example of which is the RSA (Rivest-Shamir-Adleman) protocol. The idea behind the public key cryptosystem is to use for message encryption a one-way function which is easy to compute but requires to solve a hard computational problem to find the inverse function. In the RSA protocol, such an inverse function involves the factorization of a large integer, which is hard to compute. Employing the quantum Fourier transform algorithm, Shor has shown that integer factorization becomes tractable on quantum computers, which will thus threaten the security of currently used public key cryptosystems. There is however, an alternative, absolutely secure protocol based on the private key cryptosystem, known as the one-time pad, or Vernam's cipher. In this protocol, Alice and Bob share a private key-random string of N bits known only by them. When Alice needs to communicate to Bob a secret message via public communication channel, she first converts it into ASCII binary string and then she uses the private key to encrypt the message and sends it to Bob. The encryption procedure is realized by adding the random bits of the private key, one by one, to the message string using addition modulo 2 operation. The fact that the private key string is not shorter than the message string ensures that each random bit is used only once. This guaranties absolute secrecy since the encrypted message sent through the channel does not contain any repetitive structure and is completely random. Bob, upon receiving the encrypted message, can decrypt it by binary adding the same string of random

bits of the private key. This results in undoing the encrypting transformation, and after converting the binary string into usual alphabet, Bob can read the original message. So far the cryptography protocol above is easy to perform, provided Alice and Bob share a common private key. The most difficult and costly part of the protocol is reliable private key distribution. Alice and Bob may have met before and generated the key in private. But the key should be used only once and destroyed afterwords, in order not to compromise the secrecy of communication. Once they run out of random bits, they should meet again to generate and agree on the new random string. Otherwise Alice and Bob should rely on a third party for the key distribution, but can they trust him? Fortunately, quantum information theory has found an alternative secure way of private key distribution. In fact the most advanced application of quantum information today is quantum key distribution, generally refereed to as quantum cryptography. We thus outline below three essentially equivalent protocols, demonstrating slightly different, yet complimentary aspects of quantum mechanics.

Quantum bit In classical information theory, information is usually represented in the form of classical bits, i.e. 0 and 1. For example it can be represented as an uncharged transistor ('0') and a fully charged transistor ('1'). A charged transistor can easily hold 10^8 electrons. When we consider a single particle, this situation changes. Let's think the information is stored in his internal states i.e spin. For example $s_z = -1$ represents the value '0' while $s_z = -1$ represents the value '1'. This seems the same situation as in the classical case of a transistor. However there are differences. First, the system is more sensitive to perturbations (if even a single spin value is perturbed, the information changes). Furthermore a pure qubit state can be a linear superposition of the basis states (quantum mechanic allows superposition). So the qubit can be represented like a linear combination of his basis.

$$|\psi\rangle = \alpha\,|0\rangle + \beta\,|1\rangle \tag{1.27}$$

where α and β are probability amplitudes and in general can be both complex numbers. Thanks to this property it's possible to represent simultaneously several values in a single quantum bit. For example let's think of a four qubits system. They can be in a state that is a coherent superposition of 16 different states

$$\begin{aligned} |\psi\rangle =& \frac{1}{4}\left(|0000\rangle + |0001\rangle + |0010\rangle + |0011\rangle + \right. \\ &+ |0100\rangle + |0101\rangle + |0110\rangle + |0111\rangle + \\ &+ |1000\rangle + |1001\rangle + |1010\rangle + |1011\rangle + \\ &\left. + |1100\rangle + |1101\rangle + |1110\rangle + |1111\rangle\right) \end{aligned} \tag{1.28}$$

Evidently a collection of n qubits can be in a state that is a coherent superposition of 2^n different quantum states, each of which represents a

number in binary notation. If we apply a unitary transformation of such a state, we therefore manipulate 2^n binary numbers simultaneously! This represents a massive parallelism in our computation which is responsible for the fact that a quantum mechanical system can solve certain problems exponentially faster than any classical system can do.

"No cloning theorem"[1] It's perhaps the most important quantum mechanic tool we deal with, talking about Quantum Cryptography. It states that it's impossible to create an identical copy of an arbitrary unknown quantum state. Let's think a quantum system (A), which we wish to copy $|\phi\rangle_A$. In order to make a copy we use another quantum system (B) with the same Hilbert space and blank state $|e\rangle_B$. The blank state is independent of $|\phi\rangle_A$ (which is an unknown state). A copy unitary operator acts as a copier if respects the following equation

$$U|\phi\rangle_A|e\rangle_B = |\phi\rangle_A|\phi\rangle_B \tag{1.29}$$

Now, if we apply this operator to $|0\rangle$ and $|1\rangle$ we obtain:

$$\begin{aligned} U|0\rangle_A|e\rangle_B &= |0\rangle_A|0\rangle_B \\ U|1\rangle_A|e\rangle_B &= |1\rangle_A|1\rangle_B \end{aligned} \tag{1.30}$$

Let's consider a general state

$$|\psi\rangle = \alpha|0\rangle + \beta|1\rangle \tag{1.31}$$

The linearity of U implies that

$$\begin{aligned} U|\psi\rangle_A|e\rangle_B &= U(\alpha|0\rangle_A + \beta|1\rangle_A)|e\rangle_B \\ &= \alpha U|0\rangle_A|e\rangle_B + \beta U|1\rangle_A|e\rangle_B \\ &= \alpha|0\rangle_A|0\rangle_B + \beta|1\rangle_A|1\rangle_B \end{aligned} \tag{1.32}$$

But from formula 1.29 we have

$$\begin{aligned} U|\phi\rangle_A|e\rangle_B &= (\alpha|0\rangle_A + \beta|1\rangle_A)(\alpha|0\rangle_B + \beta|1\rangle_B) \\ &= \alpha^2|0\rangle_A|0\rangle_B + \beta\alpha|1\rangle_A|0\rangle_B + \alpha\beta|0\rangle_A|1\rangle_B + \beta^2|1\rangle_A|1\rangle_B \end{aligned} \tag{1.33}$$

The only value that allows 1.32 to equal 1.33 is either $\alpha = 1$, $\beta = 0$ or $\alpha = 0$, $\beta = 1$. This is the reason why an eavesdropper can not get the photons without being discovered. But this represents also a problem if you want to exchange key over long distances and to establish a quantum type network (quantum network). In fact as for an eavesdropper is impossible to copy the quantum state without altering the properties as well as for a classical repeater is impossible to receive and retransmit a qubit without destroying the state. Because of this the maximum communication distance is limited and it is determined by the loss of channel used to transmit the qubits. At the present day, the maximum distance reached is 307 km using optical fiber[2] and 144 km using free space[3].

1.5.1 BB84

The first protocol for private key distribution was firstly suggested in 1984[4]. In this protocol Alice and Bob establish a quantum communication channel and a classical one. Alice sends photons to Bob through the quantum channel to test the presence of a possible eavesdropper between their communication channel. To do this she sends photons in one of the following states

$$\begin{aligned} |\Psi_0\rangle &= |0\rangle \\ |\Psi_1\rangle &= |1\rangle \\ |\Psi_+\rangle &= \frac{1}{2}\left(|0\rangle + |1\rangle\right) \\ |\Psi_-\rangle &= \frac{1}{2}\left(|0\rangle - |1\rangle\right) \end{aligned} \tag{1.34}$$

randomly chosen. States $|\Psi_0\rangle$ and $|\Psi_+\rangle$ correspond to the value 0 of Alice's random bit, and states $|\Psi_1\rangle$ and $|\Psi_-\rangle$ correspond to 1. Bob measures the photon states in one of the bases ($|\Psi_0\rangle$, $|\Psi_1\rangle$ and $|\Psi_+\rangle$, $|\Psi_-\rangle$), chosen at random. After the measure they use the classical channel (that can be a public one) to share what base they have used for each photon and keep just the photons for which Alice and Bob's bases were the same, discarding all the other photons. Furthermore Alice discards all the photons that, for any reason, doesn't reach Bob. After that, they share a representative sample of the photons measured on the same base and estimate the quantum bit error rate (QBER) usually due by the interaction of the photons with the environment. From the QBER estimation it is possible to quantify the maximum amount of information that may have leaked to a potential eavesdropper and remove it from the remaining photons (using amplification and error correction techniques), so to obtain a communication in which the leaked information can be kept arbitrarily low.

Now let's consider what happens when an eavesdropper, Eve, tries to infer the private key. Eve, similarly to Bob, measures the qubits in a randomly chosen basis and records the result of the measurement (but according to the no-cloning theorem, Eve can not clone the qubits). Then she has to generate each detected qubit in the measured state and send it to Bob, since otherwise Alice will discard all the lost qubits and substitute them with new ones. When Eve's basis is correct, Bob receives a qubit in the correct state. But when Eve's basis is incorrect after projecting onto the correct basis, Bob's measurement yields in a half of those cases the wrong outcome and this unavoidably increases the QBER. So if the QBER of the shared sample increases we detect the presence of an eavesdropper.

1.5.2 E92

In 1992 Bennett suggested a simplified protocol, called B92[5]. In this protocol Alice uses only two non orthogonal states, $|\Psi_0\rangle$ and $|\Psi_+\rangle$, corresponding to the values 0 and 1. Bob instead randomly decides in which base to perform the measure ($R = \{|\Psi_0\rangle, |\Psi_1\rangle\}$ or $D = \{|\Psi_+\rangle, |\Psi_-\rangle\}$). If he uses the R basis, he

assigns the value 1 to his random bits, otherwise he assigns the value 0. Furthermore Bob uses a control string where he records the measurement result, 0 for states $|\Psi_0\rangle$ or $|\Psi_+\rangle$, and 1 otherwise. That is, Bob's random bits correspond to the measurement bases, rather than to the measurement results. After this, using the classical channel he shares only the control string. In order to create a common private key, both Bob and Alice preserve the random bits that correspond to control bits having value 1, and discard all of the other bits. As before, due to low efficiency or external factors, some photons will not be detected by Bob, and Alice discards her corresponding photons too. As in BB84 protocol Alice and Bob need to sacrifice a sample of photons to calculate the QBER in order to check the presence of an eavesdropper Eve.

If Eve randomly chooses the right base she will send to Bob the correct polarization photons and he will not suspect about her presence. Nevertheless she has a 50% of possibility to choose the wrong base. In this case she will send to Bob a different photon. In a half of those cases the value result of Bob bit would be different from the Alice's one. This leads to increase the QBER value and by this info Alice and Bob will conclude that Eve is there.

1.5.3 EPR protocol

Proposed by Ekert in 1991[6], this protocol is accomplished with the help of EPR entanglement. In this case a large number of entangled qubits with states

$$|\psi\rangle_{00} = \frac{1}{\sqrt{2}}\left(|0\rangle_A |1\rangle_B + |1\rangle_A |0\rangle_B\right) = \frac{1}{\sqrt{2}}\left(|+\rangle_A |-\rangle_B + |-\rangle_A |+\rangle_B\right) \tag{1.35}$$

is shared between Alice and Bob. This could be also shared by a third part. Alice and Bob have respectively two set of measurement states $\Phi^A = (|\Psi_0\rangle, |\Psi_+\rangle, |\Psi_1\rangle)$ and $\Phi^B = (|\Psi_+\rangle, |\Psi_1\rangle, |\Psi_-\rangle)$. The measures are divided in two groups:

1. one with $\Phi_i^A \neq \Phi_j^B$
2. one with $\Phi_i^A = \Phi_j^B$.

With the first group they make a Bell's measurement to check for the presence of Eve. Like already said in section 1.3, Quantum Mechanic predicts

$$|S| = 2\sqrt{2} \tag{1.36}$$

for these set of states, instead in classical theory or LHV theory the result would be

$$|S| \leq 2 \tag{1.37}$$

Since Eve, when she performs a measure, introduces an element of reality, if $|S| = 2\sqrt{2}$ then we are sure that there isn't any eavesdropper. Instead, if we obtain $|S| \leq 2$, we will suspect about the presence of Eve. The violation of Bell's inequalities guarantees also that $E(\Phi_2^A, \Phi_1^A) = E(\Phi_3^A, \Phi_2^B) = -1$(See section 1.3). So from this relationship a random sequences of secret key can be extracted.

1.6 Quantum Dense coding

As already said above, quantum bits can carry more information with respect to the classical case. We show now how to send more than a bit of information interacting with a single qubit.

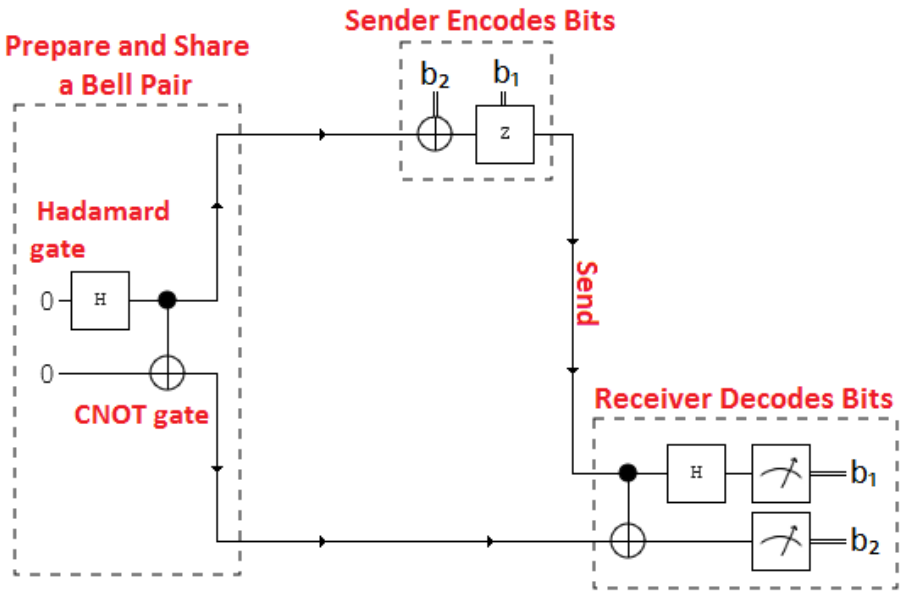

Figure 1.1: Dense coding setup

Let us think to use a pair of entangled particles. The underlying idea is that Bell's states represent an orthonormal basis and because of this, it is possible to perfectly distinguish between these states (at least neglecting experimental error). We remind that, given two photons A and B, Bell's states are defined as follows

$$\begin{aligned} \left|\Psi^{\pm}\right\rangle &= \frac{1}{\sqrt{2}}\left(\left|0\right\rangle_A\left|1\right\rangle_B \pm \left|1\right\rangle_A\left|0\right\rangle_B\right) \\ \left|\Phi^{\pm}\right\rangle &= \frac{1}{\sqrt{2}}\left(\left|0\right\rangle_A\left|0\right\rangle_B \pm \left|1\right\rangle_A\left|1\right\rangle_B\right). \end{aligned} \tag{1.38}$$

Firstly a third party send the first photon of the generated states $|\Psi^+\rangle$ to Alice and the second to Bob. Alice by performing unitary transformation on the entangled photon can change the $|\Psi^+\rangle$ state in one of the Bell's states. Then Alice sends to Bob the entangled photon, thus Bob performing a Bell measurement can distinguish in which of the different Bell states the pairs are. This can be done using a physical implementation of an Hadamard and CNOT.

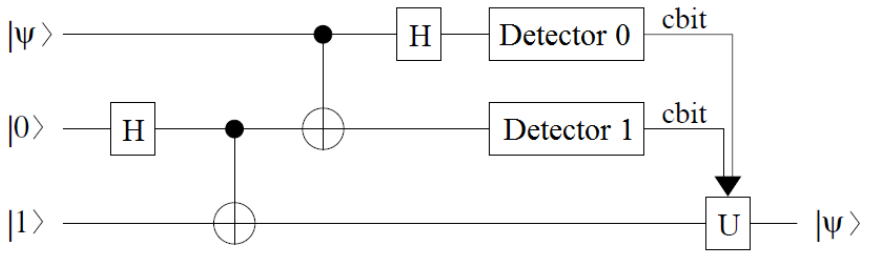

Figure 1.2: Quantum teleportation setup, the first line represents the teleported qubit. The second and third lines, after the first two gates represent the entangled pair. U, that is reached by two classical information (cbit), represents one of the four possible unitary transformation to perform, in order to get the teleported state.

The Hadamard gate, defined

$$\begin{cases} H|\Psi_0\rangle & = |\Psi_+\rangle \\ H|\Psi_1\rangle & = |\Psi_-\rangle \end{cases} \tag{1.39}$$

it's a gate that transforms the basis $\{|\Psi_0\rangle, |\Psi_1\rangle\}$ in the new basis $\{|\Psi_+\rangle, |\Psi_-\rangle\}$. Since $H^2 = I$ the inverse transformation $H^\dagger = H$.

The CNOT gate is a two qubits gate defined

$$CNOT(|x\rangle|y\rangle) = |x\rangle(|x\rangle \oplus |y\rangle) \tag{1.40}$$

where $\oplus$ represents XOR operation also on superposition states. It's easily to see that CNOT gate can generate entangled states:

$$CNOT(|0\rangle + |1\rangle)|0\rangle = \frac{1}{\sqrt{2}}(|00\rangle + |11\rangle) \tag{1.41}$$

CNOT gate is self-inverse since also $CNOT^2 = I$. So if we apply in succession a $CNOT$ and a Hadamard gates $((H \otimes I)\,CNOT)$ we can transform the Bell's states in $|00\rangle, |01\rangle, |10\rangle, |11\rangle$ that are classical bits. Practically we can successfully compress 2 bits in one qubit.

1.7 Quantum teleportation

Firstly idealized in 1993[7] and realized in 1997[8], the quantum teleportation is one of the most amazing application of quantum physics. This protocol, using 2 classical bits, can successfully send a quantum bit from Alice to Bob.

Let us consider a simple example of teleportation. Alice has a two levels system in some unknown state

$$|\varphi\rangle = \alpha|0\rangle + \beta|1\rangle . \tag{1.42}$$

She wish to send this state to Bob using only an entangled state and two bits of classical information. Even if at the beginning this seems impossible because the measurement of a qubits destroy its state. Even more this qubit hold an infinite amount of classical information because it lives in a continuous space. However this is possible if Alice and Bob share an entangled states.

$$\left|\Psi^+\right\rangle = \frac{1}{\sqrt{2}}\left(|01\rangle + |10\rangle\right) \tag{1.43}$$

Half of the entangled pair is sent to Alice and the other is sent to Bob. At this point Alice let $|\varphi\rangle$ interact with her half pairs of the entangled state. Let us consider the total state:

$$\begin{aligned}
|\chi\rangle &= |\varphi\rangle \otimes \left|\Psi^+\right\rangle \\
&= \frac{\alpha}{\sqrt{2}}\left(|001\rangle + |010\rangle\right) + \frac{\beta}{\sqrt{2}}\left(|101\rangle + |110\rangle\right) \\
&= \frac{1}{2}\left|\Phi^+\right\rangle\left(\alpha\,|1\rangle + \beta\,|0\rangle\right) + \frac{1}{2}\left|\Phi^-\right\rangle\left(\alpha\,|1\rangle + \beta\,|0\rangle\right) + \\
&+ \frac{1}{2}\left|\Psi^+\right\rangle\left(\alpha\,|0\rangle + \beta\,|1\rangle\right) + \frac{1}{2}\left|\Psi^-\right\rangle\left(\alpha\,|0\rangle - \beta\,|1\rangle\right)
\end{aligned} \tag{1.44}$$

Therefore Alice performs measurements on the Bell's basis and obtains with probability $1/4$ one of the Bell's states. So she obtains two bits of information and sends them to Bob. By this information Bob performs one of the four possible unitary transformation (I, σ_x, $i\sigma_y$, σ_z) on his qubit and recovers $|\varphi\rangle$. We note that, thanks to entanglement, local manipulations modify the whole system, no matter how distant Alice and Bob are. This is a common feature of quantum protocols.

1.7.1 Entanglement Swapping

Realized in 1998[9], this protocol, particularly similar to the quantum teleportation, has the capability to entangle particles that are generated by different sources that have never interacted before.

Let us consider two pairs of entangled particles such as

$$\begin{aligned}
\left|\Psi^+\right\rangle_{12} &= \frac{1}{\sqrt{2}}\left(|01\rangle_{12} - |10\rangle_{12}\right) \\
\left|\Psi^+\right\rangle_{34} &= \frac{1}{\sqrt{2}}\left(|01\rangle_{34} - |10\rangle_{34}\right)
\end{aligned} . \tag{1.45}$$

At this point we interact half of the first entangled pairs with the second ones and we obtain the total state

$$\begin{aligned}
|\chi\rangle_{1234} &= \frac{1}{2}\left(|01\rangle_{12} - |10\rangle_{12}\right) \otimes \left(|01\rangle_{34} - |10\rangle_{34}\right) \\
&= \frac{1}{2}\left(\left|\Psi^+\right\rangle_{14}\left|\Psi^+\right\rangle_{23} + \left|\Psi^-\right\rangle_{14}\left|\Psi^-\right\rangle_{23} + \left|\Phi^+\right\rangle_{14}\left|\Phi^+\right\rangle_{23} + \left|\Phi^-\right\rangle_{14}\left|\Phi^-\right\rangle_{23}\right)
\end{aligned} \tag{1.46}$$

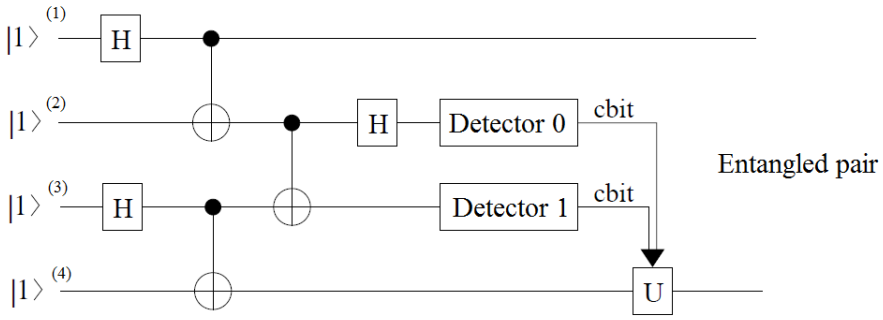

Figure 1.3: Entanglement swapping setup. The first and second lines, after the first two gates, represent the first entangled pair. Likewise the third and fourth lines after the first two gates represent the second entangled pair. Furthermore the second and third lines represent respectively the particle 2 and 3, in which we perform a measurements on the Bell's basis. The first and fourth lines represent the finals entangled pair.

Therefore if we perform a measurements on the Bell's basis of the particles number 2 and 3, the particle 1 and 4 become entangled even if they never interact. We can easily note that this protocol is archived with a similar apparatus of that of quantum teleportation, the difference consists on the fact that the particle teleported is half of an entangled pair.

Chapter 2

Hyper-Entanglement: definition and generation

In the previous chapter we have explained the great possibilities of quantum entanglement. In particular we have showed that quantum entangled states allow to increase the quantum channel capacity (Dense Coding) and we have described different QKD protocols that allow to securely share a secret key. We have also shown how entanglement can be exploited to teleport quantum states, case that is useful to entangle particles that they never interact before. In this chapter we explain what is an hyperentagled state and which physical processes are needed to produce it.

2.1 Hyperentanglement

A system is defined hyperentangled when two or more particles are entangled in more than one degrees of freedom (DOFs) that is, if given $|\phi\rangle_j$ and $|\chi\rangle_j$ that represent single particle states in the j-th degree of freedom, then we can not separate the j-th degree of freedom state $|\psi\rangle_j$:

$$|\psi\rangle_j \neq |\phi\rangle_j \otimes |\chi\rangle_j .$$

An example of hyperentangled state in polarization and time-bin DOFs is

$$|\Omega\rangle = \frac{1}{2}\left(|SS\rangle + e^{i\theta}|LL\rangle\right)\left(|HV\rangle + e^{i\varphi}|VH\rangle\right),$$

where $|H\rangle$ and $|V\rangle$ represent respectively the horizontal and vertical polarizations instead $|S\rangle$ and $|L\rangle$ represent respectively the fast and slow arrival time of the particle from the moment of generation.

2.1.1 Advantage of Hyperentanglement

Hyperentangled photons present a number of unique opportunities in quantum information processing. Firstly, they reside in an enlarged Hilbert space

compared to that of photons simply entangled (for example in polarization). For photons entangled in polarization and time-bin DOFs, the Hilbert space is $2 \times 2 \times 2 \times 2 = 16$ dimensional. In this kind of system it is relatively easy to perform quantum logic on different degrees of freedom of the same photons, as opposed to qubits residing in different photons. Consequently, hyperentanglement enables new capabilities in quantum information processing, including remote preparation of entangled states, full Bell-state analysis, and improved super-dense coding, as well as the possibility of quantum communication with larger alphabets. This is feasible because it is possible to extract information from each degree of freedom without destroying the correlation in the other degrees. This entails that working with four polarization entangled photons will give us the same information that we can get by working with two photons entangled in two different DOFs. By this information it is easy to understand that to detect N two level particles states you need at the very least N detectors (one for each particles). Instead with a hyperentangled particles you can have the same information by entangled N different degrees of freedom in the same pair of particles that needs only two detector to be revealed. So using hyperentangled quantum states it is possible to reduce the number of detector to send the same information. Furthermore the efficiency of the whole system is increased because if η represents the detection efficiency of the detector, then the efficiency of the overall system is given by η^m, where m is the number of detectors used.

Another advantage of hyperentanglement is related to the problem of decoherence. It is obviously more difficult to avoid decoherence as the number of photons increases. Alignment process is always a challenging part of quantum information experiments, and concentrating more information in a small number of particles makes experiments easier to be done. To sum up, we can say that hyperentanglement allows to simplify experiments without changing the basic ideas related with entanglement phenomena.

Super-dense Coding

The super-dense coding represents an improvement of the dense coding protocol (section 1.6). It was proposed as a solution to expand the capacity to carry information by a single particle because the linear optic doesn't permit to distinguish completely the Bell's states. However in 2008 it was demonstrated by the Paul Kwit group[10] that it's possible to improve the previous limit reached in 1995 by A. Zeilinger et al. ($\log_2 3 \approx 1.58$)[11]. The main idea behind this experiment is to code the information in more than one DOFs. Thanks to the property of hyperentangled quantum states, it is possible to perform measurements on the Bell's basis on each entangled DOFs. In theory we can code the information in four orthogonal Bell's states for each entangled DOFs. This, for an entangled states in 2 degrees, would lead a total of $4 \times 4 = 16$ different orthogonal states, so the total information that a single photon could carry is $\log_2 16 = 4$ bits. Using only linear optical instruments to distinguish Bell's states in a hyperentangled photons in polarization and OAM degrees of freedom is possible to distinguish 7

different messages. This leads to a total information of $\log_2 7 \approx 2.8$bits. It must be noted however that in the experiment of Paul Kwit group only polarization was manipulated, letting OAM states unchanged. Furthermore they didn't try to distinguish all possible messages and taking in account the experimental error a channel capacity of 1.63 was reached, effectively beating the previous record.

2.2 Non-linear Optic for Hyperentanglement

In order to generate hyperentangled photons pair, some non-linear optic processes are needed. In this section the main process involved in our experiment will be described.

2.2.1 Non-linear Optic

When we speak of linear medium, we mean a medium where the relationship between the polarization density and electric field is linear

$$P = \epsilon_0 \chi \mathcal{E} \tag{2.1}$$

where ϵ_0 is the vacuum permittivity, χ is the electric susceptibility of the medium. Instead a non linear medium has a non linear relation between P and $\mathcal{E}$. The polarization density $P = Np$ is given by the individual dipole momentum p induced by the electric field and the number density of dipole momentum N. The origin of the non linear momentum may reside either in p or in N. For example the relationship between p and $\mathcal{E}$ is linear for small electric field. But, for large displacement, the relationship between the restraining elastic force of the dipole is non linear with the displacement. Then you find that the polarization density P is a non linear function of electric field. An other way to obtain non linear behavior could reside in the number density N. Just think a laser medium where the number of atoms occupying the energy level involved in the absorption and emission of light are dependent on the intensity of the light.

Under these conditions the function P can be expanded in Taylor series about $\mathcal{E} = 0$ and by renaming the coefficient of the expansion it's found

$$P = \epsilon_0 \chi \mathcal{E} + 2d\mathcal{E}^2 + 4\chi^{(3)}\mathcal{E}^3 + \cdots \tag{2.2}$$

where the coefficient d and $\chi^{(3)}$ express the strength of the second and third-order non linear effect.

When we apply this non linear polarization density to the Maxwell's equations

$$\nabla^2 \mathcal{E} - \frac{1}{c_0^2}\frac{\partial^2 \mathcal{E}}{\partial t^2} = \mu_0 \frac{\partial^2 \mathcal{P}}{\partial t^2} \tag{2.3}$$

and conveniently writing the polarization density as a sum of a linear and non linear coefficients

$$\begin{aligned} P &= \epsilon_0 \chi \mathcal{E} + P_{NL} \\ P_{NL} &= 2d\mathcal{E}^2 + 4\chi^{(3)}\mathcal{E}^3 + \cdots \end{aligned} \tag{2.4}$$

we found

$$\begin{aligned} \nabla^2 \mathcal{E} - \frac{1}{c_0^2} \frac{\partial^2 \mathcal{E}}{\partial t^2} &= -S \\ \mathcal{S} &= -\mu_0 \frac{\partial^2 \mathcal{P}_{NL}}{\partial t^2} \end{aligned} \tag{2.5}$$

where $\mathcal{S}$ is regarded as radiation source.

2.2.2 Second-Harmonic Generation

The second-harmonic generation (SHG) is a second order non linear effect in which, by providing a harmonic electric field with frequency ω, the pumping field is splitted in two beams: one with the same frequency of the pumping electric field, the other with a double frequency. Let us consider the electrical pumping field

$$\mathcal{E}(t) = \Re\left\{E_0 e^{i\omega t}\right\} = \frac{1}{2}\left(E_0 e^{i\omega t} + E_0^* e^{-i\omega t}\right). \tag{2.6}$$

The non linear coefficient of the polarization density can be write as

$$P_{NL}(t) = d\left|E_0\right|^2 + \Re\left\{dE_0^2 e^{i2\omega t}\right\}. \tag{2.7}$$

Consequently the source $\mathcal{S}(t) = -\mu_0 \partial^2 \mathcal{P}_{NL}(t)/\partial t^2$ contains a component at frequency 2ω with complex amplitude $\mathcal{S}_{2\omega} = 4\mu_0 \omega^2 d E_0^2$ which radiates an optical field at frequency 2ω. Since the amplitude emitted is proportional to $\mathcal{S}_{2\omega}$, its intensity is proportional to $I_{2\omega} \propto \left|\mathcal{S}_{2\omega}\right|^2 \propto I_\omega^2$ whereas $I_\omega \propto \left|E_0\right|^2$. Since the emissions are added coherently the intensity of the second-harmonic wave is proportional to the square of the length of the interaction volume L.

By these information it's possible to affirm that the efficiency of the second-harmonic generation is

$$\eta_{SHG} = \frac{I_{2\omega}}{I_\omega} = C^2 L^2 I_\omega = C^2 \frac{L^2}{A} P \tag{2.8}$$

where P is the incident power of the wave, A is the cross-section area of the interaction volume and C^2 is a constant proportional to d^2 and ω^2.

2.2.3 Spontaneous Parametric Down Conversion

The spontaneous parametric down conversion[12] (SPDC) is a three-wave mixing process where there is only a single input wave and the downconversion at lower frequency is spontaneous, that is stimulated by vacuum random fluctuations.

In particular the Type-II SPDC is the most important tool to generate entangled photons. The basic idea is that the incoming photon is spitted into two photons, labeled by e and o, which are entangled in different DOFs. To be able to allow this phenomena, energy and momentum (phase-matching) must be conserved. In Type-II crystal, the process is summarized as

$$e \to e + o \tag{2.9}$$

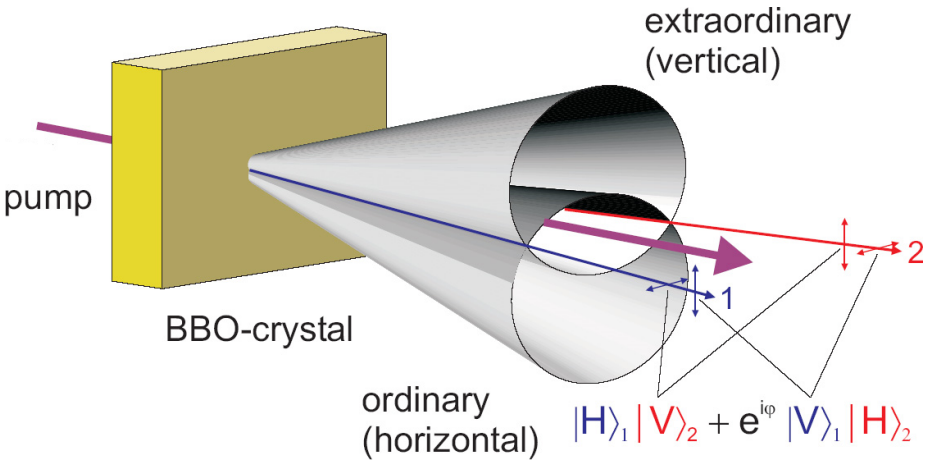

Figure 2.1: BBO and circles generated by SPDC process. The polarization entangled photons are located in the intersection between the two circles. In the intersection one does not know which photon will be H or V

this implies that the emitted downconverted photons must lie on two shifted crossing circles with horizontal and vertical polarization (see figure 2.1). Let us consider the amplitude to detecting photons pair at conjugate space-time points $(\vec{r}_1, t_1)$ and $(\vec{r}_2, t_2)$ is given by

$$A = \left\langle \vec{E}_H^{+}(\vec{r}_1, t_1)\, \vec{E}_H^{+}(\vec{r}_2, t_2) \right\rangle \tag{2.10}$$

where $t_1$and t_2 represent the detection time and $\vec{E}_H^{+}(\vec{r}_i, t_i)$, $(i = 1, 2)$ are the Heisenberg electric field operators. In the steady state the right-hand-side of amplitude it can be expressed as

$$A \propto \int d^3r_3 \int d^3k_1 \int d^3k_2 U^{\star}_{\vec{k}_1\lambda_1}(\vec{r}_3) U^{\star}_{\vec{k}_2\lambda_2}(\vec{r}_3) U_{\vec{k}_0\lambda_0}(\vec{r}_3) f_p(\vec{r}_3) \left(\frac{\hbar\omega_{k_0}}{2\varepsilon_0}\right)^{\frac{1}{2}} \left(\frac{\hbar\omega_{k_1}}{2\varepsilon_0}\right)^{\frac{1}{2}}$$
$$\left(\frac{\hbar\omega_{k_2}}{2\varepsilon_0}\right)^{\frac{1}{2}} \times \langle a_{k_0}, 0|\, \vec{E}_I^{(+)}(\vec{r}_2, t_2)\, \vec{E}_I^{(+)}(\vec{r}_1, t_1)\, |a_{k_0}, k_1, k_2\rangle\, \delta(\omega_{k_1} + \omega_{k_2} - \omega_{k_0}) \tag{2.11}$$

where $\vec{E}_I(\vec{r}_i, t_i)$, $(i = 1, 2)$ are the interaction-picture electric field operators and $f_p(\vec{r}_3)$ is a function which describes the shape of the pump in the transverse direction. $U_{\vec{k}_0\lambda_0}(\vec{r}_3)$, $(i = 0, 1, 2)$ are plane-wave modes describing the electromagnetic field in free space with $\vec{k}_1, \vec{k}_2$ as the wave vectors of the signal and idler photons, $\vec{k}_0$ is the wave vector of the incident pump photon and λ_i are polarization indices. The initial state of the electromagnetic field $|0, a_{k_0}\rangle$, consists of a coherent state with wave-vector $\vec{k}_0$ and frequency ω_0 (the monochromatic pump beam) with other modes in the vacuum state $|0\rangle$. The electric fields of

the downconverted pair are given by

$$\begin{aligned}\vec{E}_I^{+}\left(\vec{r}_1,t_1\right) &= \frac{1}{\sqrt{2}}\left[\vec{E}_{I,o}^{+}\left(\vec{r}_1,t_1\right)+\vec{E}_{I,e}^{+}\left(\vec{r}_1,t_1+\tau\right)\right]\\ \vec{E}_I^{+}\left(\vec{r}_2,t_2\right) &= \frac{1}{\sqrt{2}}\left[\vec{E}_{I,o}^{+}\left(\vec{r}_2,t_2\right)+\vec{E}_{I,e}^{+}\left(\vec{r}_2,t_2+\tau\right)\right]\end{aligned} \tag{2.12}$$

where $\vec{E}_{I,o}^{+}, \vec{E}_{I,e}^{+}$ are the electric fields for ordinary and extraordinary photons respectively. The interaction-picture quantized electric field $\vec{E}_I^{(+)}\left(\vec{r},t\right)$ is given as

$$\vec{E}_I^{+}\left(\vec{r},t\right) = i\sum_{\lambda}\int d^3k\left(\frac{\hbar\omega_k}{2\varepsilon_0}\right)^{\frac{1}{2}}\varepsilon_{\vec{k}\lambda}e^{i\left(\vec{k}\vec{r}-\omega t\right)}a_{\vec{k}\lambda} \tag{2.13}$$

where $a_{\vec{k}\lambda}$ is the annihilation operator for photons with wave vector $\vec{k}$ and λ is the polarization index; $\vec{\varepsilon}_{\vec{k}\lambda}$ $(\lambda=1,2)$ denote the mode polarization vector. We assume that the divergence of the pump is negligible over the length of the crystal and that the transverse shape of the pump is Gaussian

$$f_p(\vec{r}_3) \propto e^{-\left(\frac{r_{3x}^2+r_{3y}^2}{\varepsilon_\perp^2}\right)} \tag{2.14}$$

The plane-wave mode functions are given as $U_{\vec{k}_j\lambda_j}(\vec{r}_3) = e^{\left(-i\vec{k}_j\vec{r}_3\right)}$. After performing the $\vec{r}_3$ integration in formula 2.11 and using the transformations in formula 2.12 we obtain

$$\begin{aligned}A \propto \int\int d\omega_{k_1}d\omega_{k_2}sinc\left(\Delta k\frac{d}{2}\right)\Big[&e^{i\left(\vec{k}_1\vec{r}_2-\omega_1t_2\right)}e^{i\left(\vec{k}_2\vec{r}_1-\omega_2(t_1+\tau)\right)}\\ -&e^{i\left(\vec{k}_1\vec{r}_1-\omega_1t_1\right)}e^{i\left(\vec{k}_2\vec{r}_2-\omega_2(t_2+\tau)\right)}\Big]\delta\left(\omega_{k_1}+\omega_{k_2}-\omega_{k_0}\right)\end{aligned} \tag{2.15}$$

where $\vec{k}_1, \vec{k}_2$ are the wave vectors of the ordinary and extraordinary photons respectively, d is the length of the non linear crystal and $\Delta k = k_0 - k_1 - k_2$. The two-photons state has a finite bandwidth so we let $\omega_{k_1} = \omega_{k_1^\star} + \nu$ and $\omega_{k_2} = \omega_{k_2^\star} - \nu$ where $|\nu| \ll \omega_{k_{1,2}^\star}$ and $\omega_{k_{1,2}^\star}$ are phase-matched frequencies of the signal and idler photons. Expanding k_1 and k_2 to first order in ν we obtain

$$\begin{aligned}k_1 &= k_1^\star + \nu/u_0\\ k_2 &= k_2^\star + \nu/u_e\end{aligned} \tag{2.16}$$

where $u_o(u_e)$ is the group velocity for the ordinary (extraordinary) photons. If we consider the degenerate case in which $\omega_{k_{1,2}^\star} = \frac{\omega_{k_0}}{2}$ and we use the delta function in equation 2.15 together with the dispersion relations for the wave numbers in 2.16 we obtain, after integrating over all t_1 and t_2, the modulus square of A proportional to the following integral

$$|A|^2 = \int d\nu\, sinc^2\left[\tau_1\nu\right]\left(1-\cos\left(2\nu\left[\tau+\tau_2\right]\right)\right) \tag{2.17}$$

where

$$\tau_1 = \left(\frac{1}{u_0} - \frac{1}{u_e}\right)\frac{d}{2} \, and \, \tau_2 = \left(\frac{1}{u_0} - \frac{1}{u_e}\right) z \tag{2.18}$$

and we have assumed that each detector is of equal distance z from the center of the non linear crystal. Note that, polarization entangled photons are generate in the crossing points of the two circles. In fact, the incoming photons of the ordinary and extraordinary waves have horizontal and vertical polarization respectively. In the intersections we will find either horizontal or vertical polarized photons however it is not possible to know where we will find one or the other until we measure the photons polarization. Hence through SPDC process, we have generated the polarization entangled state

$$|\Psi\rangle = \frac{1}{\sqrt{2}}\left(|HV\rangle + e^{i\varphi}|VH\rangle\right) \tag{2.19}$$

Chapter 3

Entanglement loophole

When a Bell's measure is performed, for practical reasons some loopholes are permitted. These loopholes refer to circumstances in an experiment that force us to make extra assumptions for the test to apply. Such a loophole can be used to avoid the law without technically breaking it.

The Bell inequality is derived under the assumption of local realism and it is violated by quantum-mechanical predictions, and therefore local realist models cannot give quantum-mechanical predictions. However, during an experiment, we are no longer in the ideal setting of the Bell theorem. There are unintended and unexpected circumstances that open possibilities for local realism to give the output of the experiment, circumstances that constitute loopholes in Bell inequality tests. Then in this chapter we show some of the main loopholes and the one that we have verified.

3.1 "Locality" loophole

Firstly presented by Bell in 1964[13], this loophole comes from the fact that locality is an explicit assumption made to derive the Bell inequality. If communication between the sites is possible (so that locality is not enforced), then local hidden variables models are possible. For example this happens when measurement settings are chosen and set long before an experimental run. Under these circumstances there is nothing that prevents a signal from traveling from one site to another and that signal can carry influence from the remote setting to the local outcome. All these highlight the importance of changing the measurement settings quickly. The first experiment to close the locality loophole was performed by Aspect, Dalibard, and Roger in 1982[14]. In their experiment the distance from each measurement site to the source was 6 meters, or 20 ns. The settings were switched every 10 ns, and the coincidence window used was 18 ns, closing the locality loophole as already stated.

3.2 "Efficiency" loophole

Reported by Pearle in 1970[15], this represents a very delicate problem, yet one of great importance. In an ideal experiment every experimental run is concluded with a detection in the measurement system. Instead in a real experiment this is not true. The main causes of this behavior are that:

- if there are losses in the experimental setup then the particles could never reach the receiver,
- even the receiver has their own efficiency of detection, so one or both the particles of a entangled pair could be lost. Since there may be no indication of this in the experiment, there could be no corresponding event recorded in the experimental data.

This unexpected circumstance makes the original Bell inequality derivation invalid.

The first experiment to close the efficiency loophole was performed by Rowe in 2001[16]. In his experiment he used two ions in a trap and every experimental run gives output data, so it is free of the efficiency loophole. Sadly the ions are 3 µm apart while a measurement lasts 1 ms, so the experiment own the locality "loophole". A more recent experiment performed in 2015 employs an event-ready scheme that enables the generation of high-fidelity entanglement between distant electron spin (a spatial separation of 1.3 km) and this represent the first loophole-free violation of a Bell inequality.[17]

3.3 "Post selection" loophole

This represents the loophole that we have tested during the thesis in order to verify if a local realist model with long realist delays can describe the physical results of time-bin entangled photons. To create a time-bin entangled pair we need to use an unbalanced Michelson interferometer where the path difference is larger then the coherence length, before the SPDC crystal. In this way we create a two levels system with two detection events: one at the "early-setting readoff" event for the early detection, and one at the "late-setting readoff" event for the late detection. In order to make indistinguishable the two levels, at the measure side, two other interferometers with the same path difference must be used: one for Alice and one for Bob (see figure 3.1). In this kind of setup, even in the ideal case of two-particle with enough spatial separation between the local measurements (which closes the locality loophole), and perfect detection efficiency (which closes the detection loophole), there are local hidden variable models that reproduce the quantum predictions for the violation of the CHSH inequality. This happen because in our setup, the detection of a coincidences event (two photons that are detected at the same time) could depend on local setting.

To show this we use the local hidden variables model introduced in 1999 by Aerts et al.[18]. Their model need two hidden variables: an angular coordinate

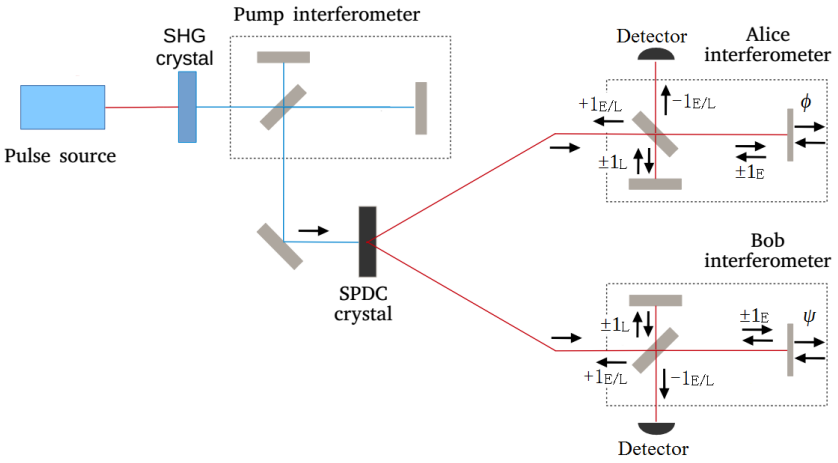

Figure 3.1: Generic setup to create and measure a time-bin entangled source. ϕ and ψ represent the shifts introduced by the local setting on Alice and Bob interferometer. They can be controlled moving the position of the mirrors of some nanometers on the long arms of the Alice/Bob interferometers as shown in figure. $+1_{E/L}$ represent the early and late events that after have chosen the short or long path in the first passage through the beam splitter, during the second one have chosen the path that leads to the SPDC crystal. Instead $-1_{E/L}$ represent the early and late events that after have chosen the short or long path in the first passage through the beam splitter, during the second one have chosen the path that leads to the detector. Since this setup use a Michelson interferometer, only -1_X events can be detected, if instead we use a Mach-Zehnder interferometer, then we can detect both $+1_X$ and -1_X. $\pm1_E$ and $\pm1_L$ represent respectively the early and late event before the second passage through the beam splitter. If we reject each pairs of events whose registration times differ by the time delay between the short and long light path of the interferometers then we are sure that early events have chosen the long arm of Alice/Bob interferometers and the late events have chosen the short arm of Alice/Bob interferometers.

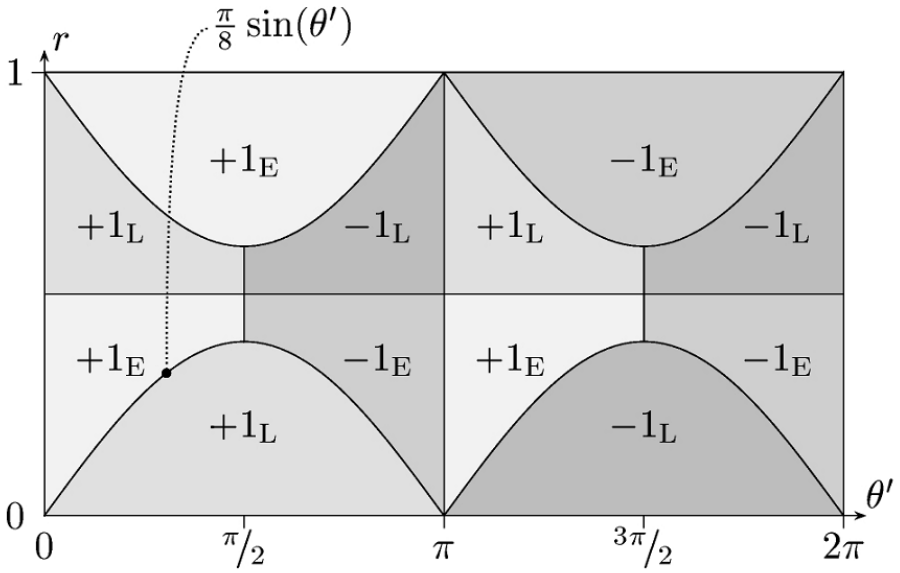

Figure 3.2: LHV model for Alice detector. The shifted value of the angular hidden variable, $\theta' = \theta - \phi$, and r, determine if the particle are revealed (-1) or it's sent back to the SPDC crystal (+1), and whether the particle is detected early E or late L. The lower curve in the left side of the chart is given by $\frac{\pi}{8}\sin\theta'$, and the shape of the other curves are of similar form. To be noted that the symbols have the same meaning as in figure 3.1

$\theta \in [0, 2\pi]$ and an additional coordinate $r \in [0, 1]$. This variable are uniformly distributed in (θ, r). Each pair of entangled particles is then described by a definite point (θ, r). On Alice detector, the measurement results are decided by the hidden variables (θ, r) and the local setting (ϕ) of the apparatus that is the phase introduced by Alice's interferometer. When a photon pass through the interferometer the variable θ is shifted by the local setting ($\theta' = \theta - \phi$). The results of the measurement are read off in figure 3.2. Likewise on Bob detection a shift is introduced ($\theta'' = \theta + \psi$, where ψ is the phase introduced by Bob interferometer). In figure 3.3 is shown the results obtained during a measure. The single-particle detection probabilities follow the predictions of Quantum Mechanics since in figures 3.2 and 3.3 all the possibility have the same probability. The coincidence probabilities are determined by overlapping the two figures 3.2 and 3.3 with the proper shifts. We now provide the estimate of the expectation values of the net coincidence probability:

$$\begin{aligned} P(-1;-1(coinc)|\phi,\psi) &= P(-1_E;-1_E|\phi,\psi) + P(-1_L;-1_L|\phi,\psi) \\ &= \frac{2}{2\pi}\int_0^{\psi+\phi}\frac{\pi}{8}sin(\theta)d\theta = \frac{1}{8}[1-cos(\psi+\phi)] \end{aligned} \tag{3.1}$$

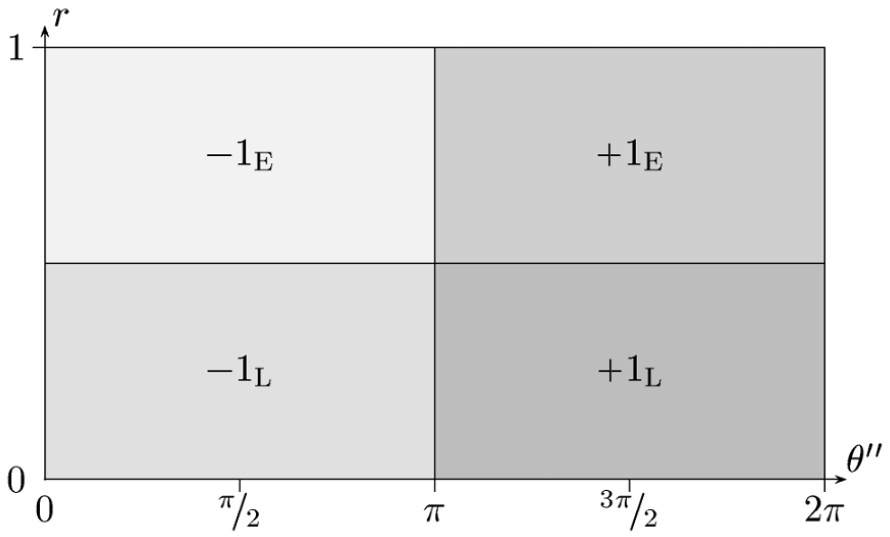

Figure 3.3: The measurement result at the Bob detector as a function of the shifted hidden variables. The symbols have the same meaning as in figure 3.2.

where E and L subscripts represent respectively the early and late coincidences. It is easy to verify that this model also gives the correct prediction for the other detection events. Using this model let us see what happen when we perform a Bell inequality. To study this model we introduce the following parameters: t_d that is the detection time, t_{ret} that is the time in which light reaches the detector from the location of the phase shifter (interferometer), $\Delta\mathcal{T}$ that is the time delay between the short and long light path of the interferometer. Each pairs of events whose registration times differ by $\Delta\mathcal{T}$ are rejected, moreover each pairs of events which do not have the feature that the phase setting at $t_d - \Delta\mathcal{T} - t_{ret}$ was ϕ_0 on Alice detector and ψ_0 on Bob detector. If we discard the latter event we ensure that the hypothetical LL subensemble within the remaining data is independent of the phase settings at $t_d - t_{ret}$. Then, if local realism holds, the Bell CHSH inequality applies to this LL subensemble

$$|E_{LL}(\phi_1, \psi_1) + E_{LL}(\phi_2, \psi_1) + E_{LL}(\phi_2, \psi_2) - E_{LL}(\phi_1, \psi_2)| \leq 2 \tag{3.2}$$

where the phase are taken at $t_d - t_{ret}$. This is valid since each of the correlation functions is an average on the same ensemble. If the ensemble is a function of the phase settings $t_d - t_{ret}$, then the bound would be higher. Indeed, the remaining EE subensemble may still depend on the phase setting at $t_d - t_{ret}$ even after this selection, and we only have

$$|E_{EE}(\phi, \psi)| \leq 1. \tag{3.3}$$

Of all events that submit this inequality, again half are EE and half are LL, so that

$$E_{coinc.}(\phi,\psi)=\frac{1}{2}E_{EE}(\phi,\psi)+\frac{1}{2}E_{LL}(\phi,\psi) \tag{3.4}$$

thus we found that the outcomes of the module of S parameter (see formula 1.8) for a local realist model with long realist delays obey

$$|S|\leq\frac{1}{2}(2+4)=3 \tag{3.5}$$

where the bounds 4 represent the early coincidences and the bound 2 represent the late coincidences. But this is larger than the maximal quantum prediction $2\sqrt{2}$. To establish a better bound we need to use the so-called "chained" Bell inequalities.

3.3.1 "Chained" Bell inequality

The "chained" Bell inequality is a "chained" extension of the Bell-CHSH inequality. For example if we calculate the bound for a Bell inequality at 6 parameters for a local realist model regarding the LL subensemble is

$$\begin{aligned}&|E_{LL}(\phi_1,\psi_1)+E_{LL}(\phi_2,\psi_1)+E_{LL}(\phi_2,\psi_2)+E_{LL}(\phi_3,\psi_2)\\&+E_{LL}(\phi_3,\psi_3)-E_{LL}(\phi_1,\psi_3)|\leq 4\end{aligned} \tag{3.6}$$

If local realism holds formulas 3.3, 3.4 and 3.6 suggest that

$$\begin{aligned}&|E_{coinc}(\phi_1,\psi_1)+E_{coinc}(\phi_2,\psi_1)+E_{coinc}(\phi_2,\psi_2)+E_{coinc}(\phi_3,\psi_2)\\&+E_{coinc}(\phi_3,\psi_3)-E_{coinc}(\phi_1,\psi_3)|\leq\frac{1}{2}(4+6)=5\end{aligned} \tag{3.7}$$

Again the bound is the mean value of the trivial bound 6 for the early coincidences and 4 for the late coincidences. Now we consider the following 6 directions $\pi/6$ apart in a plane

ϕ_1	0	ψ_1	$\pi/6$
ϕ_2	$-\pi/3$	ψ_2	$\pi/2$
ϕ_3	$-2\pi/3$	ψ_3	$5\pi/6$

using the quantum mechanic we obtain

$$\begin{aligned}&|E_{coinc}(\phi_1,\psi_1)+E_{coinc}(\phi_2,\psi_1)+E_{coinc}(\phi_2,\psi_2)+E_{coinc}(\phi_3,\psi_2)\\&+E_{coinc}(\phi_3,\psi_3)-E_{coinc}(\phi_1,\psi_3)|=\\&|\cos(\pi/6)+\cos(\pi/6)+\cos(\pi/6)+\cos(\pi/6)+\cos(\pi/6)\\&-\cos(5\pi/6)|=6\cos(\pi/6)\approx 5.20>5\end{aligned} \tag{3.8}$$

Because no local realist model with long realist delays give a value greater than 5, with this it is possible to perform a test. So, even if the standard Bell inequalities are not sensitive enough to show a violation of local realism

in the experiment, because their bound is raised by the noise introduced by the early-early subensemble, using a "chained Bell inequality" a violation of the local realism can be found even with this noise included. However, this violation is minimal, therefore a measure with high visibility is needed. To solve this problem, studying the "chained" Bell inequality at a greater number of parameter[19] like the previous steps, we found

# of parameters	Realism bound	Quantum prediction	Critical visibility
4	3	$4\cos(\pi/4) \approx 2.828$	$> 100\%$
6	5	$6\cos(\pi/6) \approx 5.196$	96.23%
8	7	$8\cos(\pi/8) \approx 7.391$	94.71%
10	9	$10\cos(\pi/10) \approx 9.511$	94.63%
12	11	$12\cos(\pi/12) \approx 11.59$	94.90%
$2N \geq 14$	$2N-1$	$2N\cos(\pi/(2N))$	incr. with N

It's easy to understand that considering the visibility, the best conditions in order to violate "chained" Bell inequality are met using 10 parameters.

Chapter 4

Experimental Setup

In this experiment we want to create an hyper-entangled state in time-bin e polarization degrees of freedom. As we explain in the previous chapters, to ensure this result we use a Michelson interferometer and a type II spontaneous parametric down conversion process. Since we want to perform a "chained" Bell measurement and a tomography measurement on a free-space channel we need a pair of polarimeters and Michelson interferometers which can manipulate the polarization and time-bin degrees of freedom as well as a free space channel. This last part is explained in this and 5 chapters.

The experimental setup (figure 4.1) is composed of:

Laser Source

Mira-HP Coherent is a commercial ultrafast Ti:Sapphire oscillator (figure 4.2). It works at an average power of $3.5\,W$ in femtosecond mode and can also work at picosecond mode. Furthermore it has a tunable wavelength and it is designed specifically to be pumped by the Verdi G18 laser. Verdi G18 Coherent is a continuous wave green pump laser that uses a semiconductor chip as the active medium in place of a conventional laser crystal. The oscillating wavelength is $1064\,nm$ intracavity doubled to produce a $532\,nm$ green output beam. It has a spectral purity higher than $99\,\%$, an output power of $18\,W$, a linear vertical polarization and a spatial mode TEM_{00}. The following table reports the Mira-HP characteristics working at $800\,nm$ when pumped with Coherent Verdi G18 laser (figure 4.2). In our experiment the Mira-HP is used at a wavelength of $808\,nm$ in femtosecond mode principally to increase the SHG efficiency. As shown later this is also useful because working in femtosecond mode, the difference length of the two arms of the interferometers to produce the time-bin entangled pairs is limited.

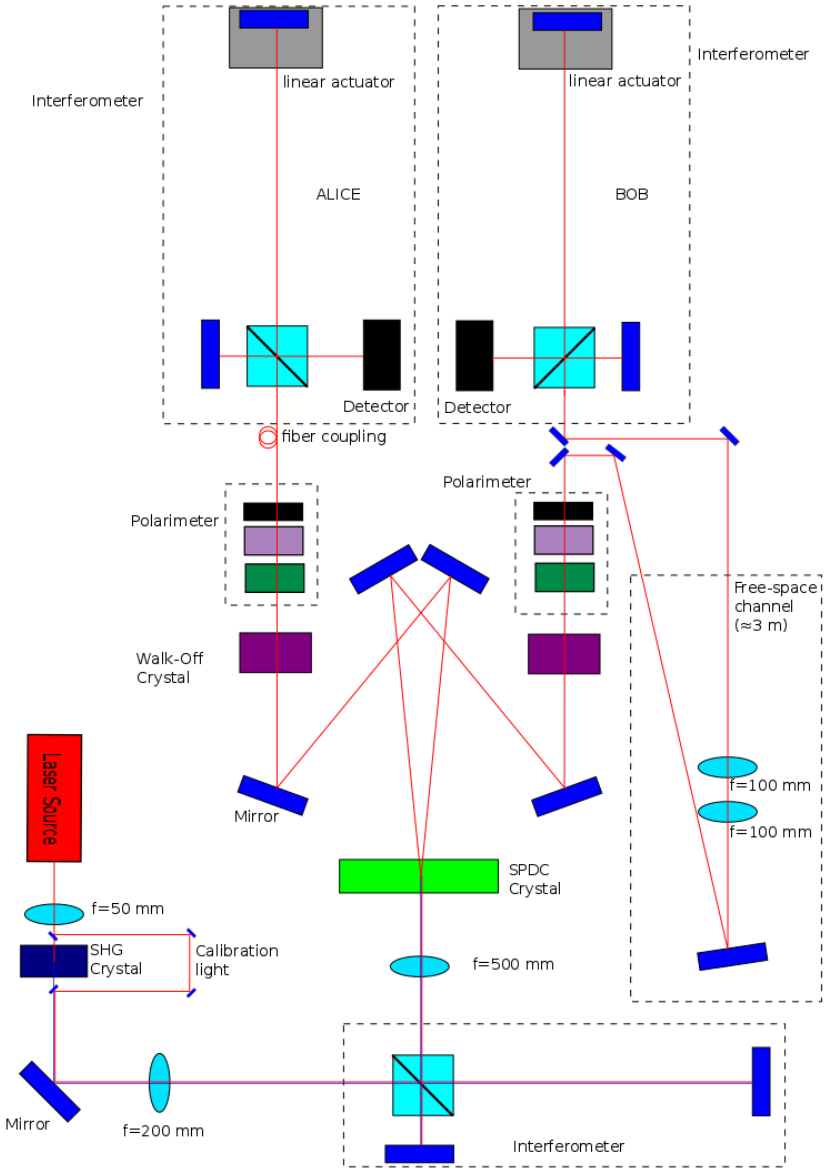

Figure 4.1: Setup of the hyperentanglement source in time-bin and polarization DOFs. The red line represents photons with wavelength at 808nm instead the blue line represents photons at 404 nm.

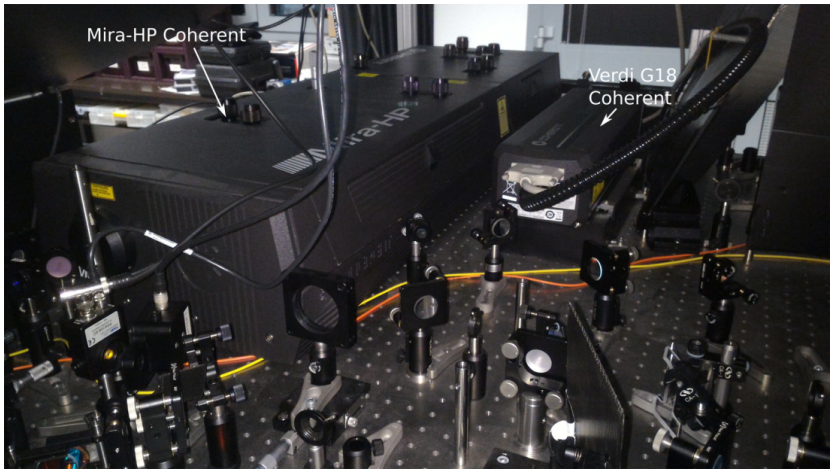

Figure 4.2: Laser source. On the left we can see the Mira-HP Coherent Laser, on the right we found Verdi G18 Coherent Laser source.

Output Power	>3.5
Pulse Width	<130 fs
Tuning Range (nm)	700 to 1000
Repetition-Rate (MHz)	76
Noise (%)	<0.1
Stability (%)	<3
Beam Diameter (mm)	0.8
Beam Divergence (mrad)	1.5
Spatial Mode	TEM_{00}
Polarization	Horizontal

Table 4.1: Mira-HP Characteristic

SHG Crystal

Since the semiconductor detectors have a high efficiency around 800 nm a BiBo crystal is used as Second harmonic generation. By this crystal we obtain $404\,nm$ photons that after the SPDC crystal become at $808\,nm$. In order to increase the conversion efficiency (formula 2.8) we reduce the cross area of the active volume focalizing the laser beam using a lens with 75mm of focal. The SHG efficiency is found to be about $\eta_{SHG} \approx 37\%$. Since there isn't an unitary efficiency, we collect this light and apply a delay so that can be time distinguished from the entangled light. We call this light calibration light and it's used in order to stabilize the interferometer.

Pump Michelson Interferometer

An unbalanced Michelson's interferometer (figure 4.3) is used to create the time-bin entangled photons. In order to create the time-bin entangled photons, we need to create a time indetermination of the pulse position. This is done by strongly unbalanced Michelson's interferometer. To be sure to generate a two levels system, the path difference of the interferometer must be longer than the pulse length in order to avoid a single-photon interference. After the interferometer we obtain photons in the state

$$|\varphi\rangle = \frac{1}{\sqrt{2}}\left(|S\rangle + e^{i\phi}\,|L\rangle\right) \tag{4.1}$$

where $|S\rangle\ and\ |L\rangle$ represent the short and the long path respectively and $\phi = 2\pi\frac{D-d}{\lambda}$ where $D\,and\,d$ indicate the long and the short path length and λ represents the wavelength of the beam. All this is placed after a lens with $200\,mm$ focal which is useful to increase the Rayleigh range so that the width of the beam that follows the long arm and the one that follows the short arm are very similar. This property guarantees that the power measured by the beam which follows the long arms is equal to the beam which follows the short arm. It can be noted using the information that we get until now that a path difference between the two arms, greater that $39\,\mu m$ is enough to be sure that there isn't single-photon interference. However this can not be distinguished by our detectors and electronics, so a path difference of $50\,cm$ is used.

SPDC crystal

The SPDC crystal (see figure 4.4) is a BBO crystal which allows the Spontaneous Parametric Down Conversion by which we obtain the hyperentangled pair. The beam is focalized on the crystal with a $500\,mm$ focal lens. It splits the incoming photon in two photons transforming the initial state in equation 4.1 in a state entangled in different degrees of freedom. Among the different DOFs we take

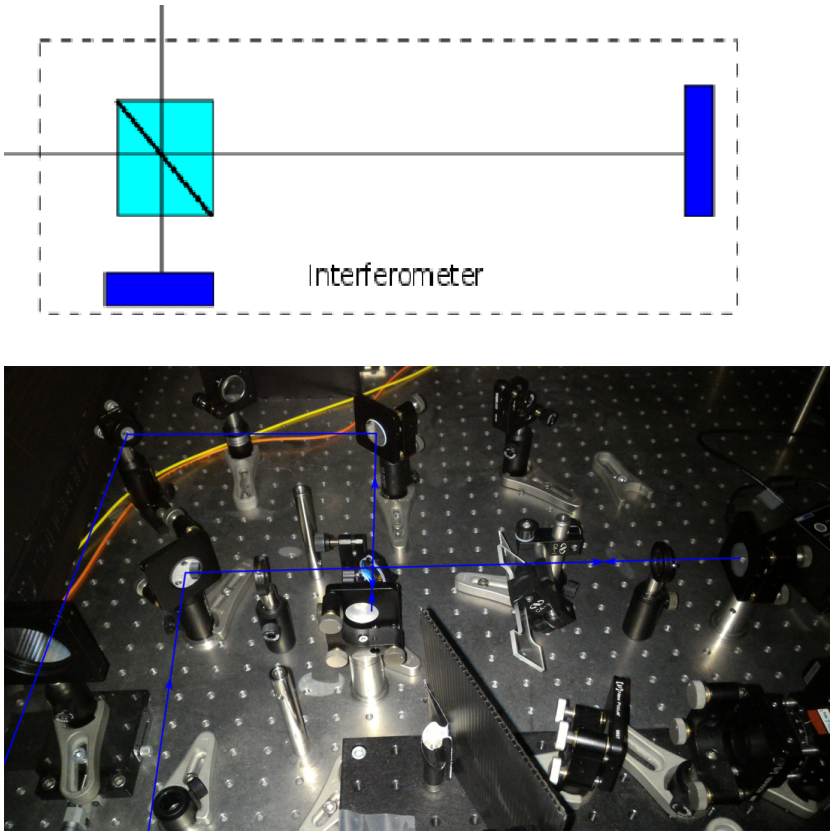

Figure 4.3: The top image shows a Michelson's Interferometer scheme. The bottom image represents its implementation.

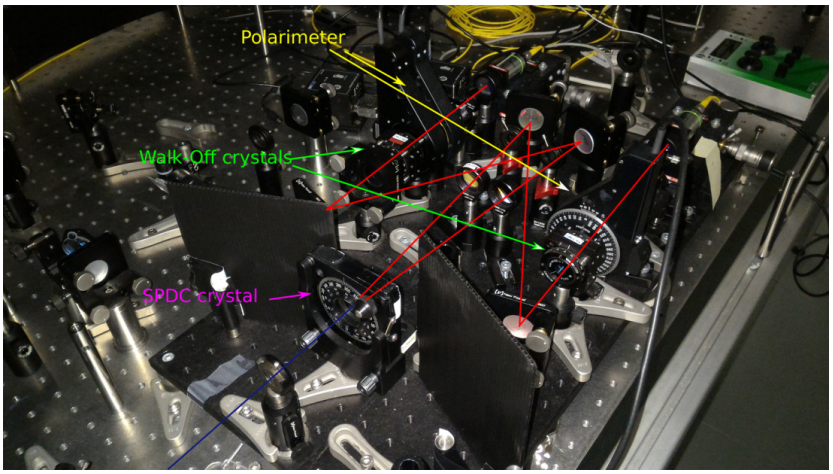

Figure 4.4: In this image we can see the SPDC crystal, the walk off crystals, and the polarimeters. The blue and red lines represent respectively the photons at 808 nm and 404 nm.

advantage of polarization (see section 2.2.3) and we obtain

$$|\Xi\rangle = \frac{1}{2}\left(|S\rangle_A |S\rangle_B + e^{i\phi} |L\rangle_A |L\rangle_b\right) \otimes \left(|H\rangle_A |V\rangle_B + e^{i\varphi} |V\rangle_A |H\rangle_b\right) \qquad (4.2)$$

Walk-Off crystal

Since BBO is a birefringent crystal, different polarizations get different delays. This represents a problem because the BBO crystal length is enough to introduce a delay between the polarizations greater than the coherence length of the impulse ($39\,\mu m$). Thanks to this it's possible to distinguish the different polarization states and this destroys the entangle states. To get over this difficulty, we insert, after SPDC, on both channels, a Walk-Off Crystal (figure 4.5). The Walk-Off crystal (see figure 4.4) is practically another BBO crystal with half length of the SPDC crystal that is rotated of 90° respect to the BBO crystal in order to invert the ordinary and extraordinary axes. The half length is due to the fact that the incoming photons split, at half of the SPDC crystal on average. The inversion of the ordinary and extraordinary axes is done in order to correct the initial delay.

Polarimeter

In order to verify the produced polarization entangled state we need an instruments that is able to perform measures of photons at several polarization states. To measure the polarization we use a polarizing beam splitter (PBS) that divides the incoming beam in two beams: one with horizontal polarization and

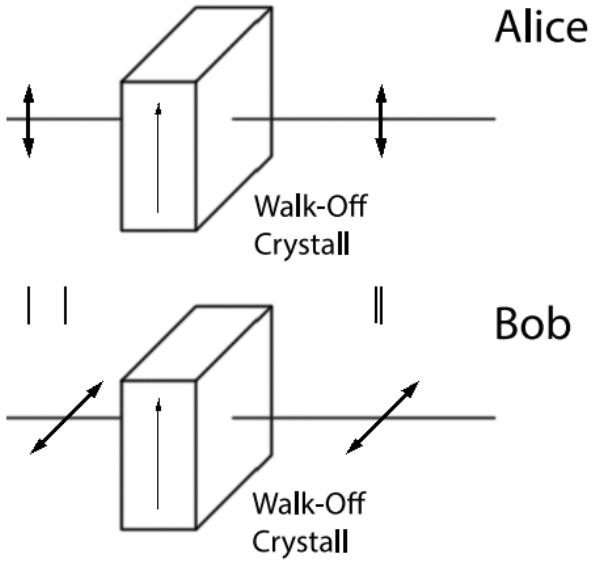

Figure 4.5: Correction obtained with Walk-Off Crystals.

one with vertical polarization. Furthermore in order to measure other type of polarization before the PBS a $\frac{\lambda}{4}$ and a $\frac{\lambda}{2}$ wave plates are used to convert all the possible polarization states in vertical polarization states (see sec. 5.1). Using a motorized rotation stage PRM1Z8 of Thorlabs (see image 4.4) the axes of the just mentioned plates are rotated to the desired position in order to find the wanted stage.

Free-space channel

To simulate a free-space propagation of the photons sent to Bob, we create a free space channel (figure 4.6) using some mirrors, in order to create a long light path maintaining small size of the device. A set of two lens are used to ensure a good focalization of the beam when it reaches the Bob detector.

Alice and Bob Michelson Interferometers

In order to measure different type of time-bin entangled states two unbalanced Michelson's interferometers are used to project the state in the wanted basis (figure 4.8). The path differences must be the same of the first interferometer at least of the coherence length of the laser impulse. The length of the long

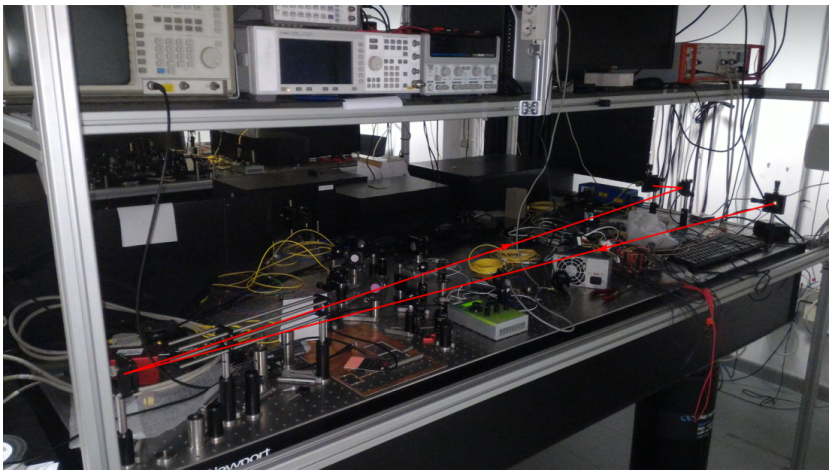

Figure 4.6: Free-space channel

arms are controlled using two SmarAct linear actuator that allow nanometric movements coupled with two Modular Control Systems (MCS).

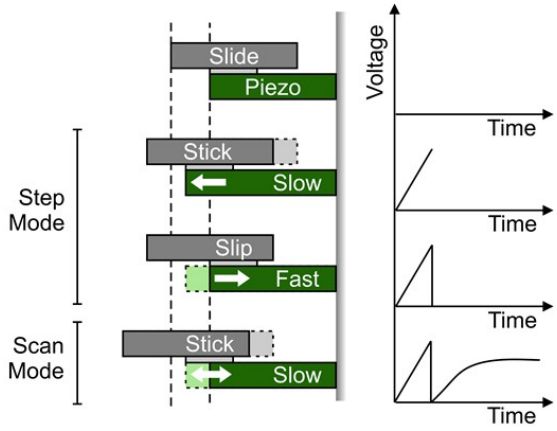

Figure 4.7: Linear actuator driving principle.

The linear actuators use the stick-slip principle (figure 4.7) to perform fine steps down to 50 nm (step mode). Moreover, with a slow elongation of the piezo element the slide can be moved with sub-nanometer resolution within a range of about 1.4 µm by default and up to several µm on request (scan mode). Furthermore the light passing through the long e short arms can be stopped in order to select the light coming only by one arm. This, as explained in sec. 5.2 and 5.3, can be used to project the time-bin entangled state in a selected state and retrieve the result.

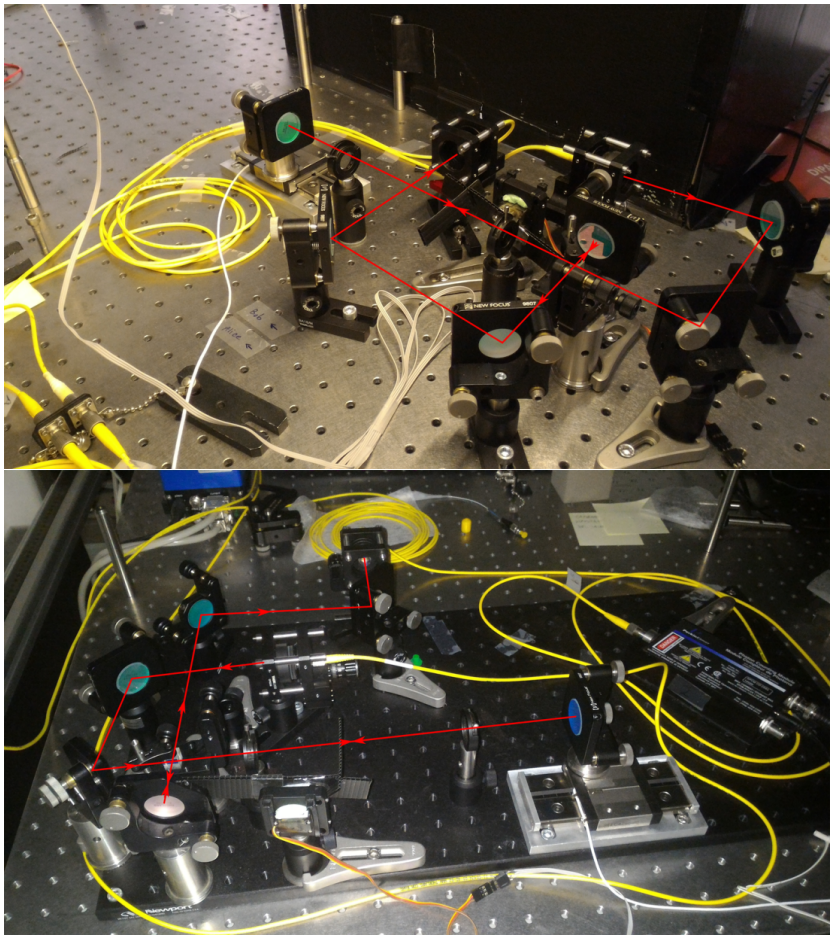

Figure 4.8: Alice(on top) and Bob(bottom) Michelson Interferometers

Detector

In order to detect the single photons, Single Photon Avalanche Diodes (SPAD) are used, provided by Excelitas SPCM-AQRH, Single Photon Counting Module. It uses a unique silicon avalanche photodiode, achieving a peak photon detection efficiency greater than 70% at 700nm over a 180µm diameter with uniformity over the full active area. A TTL level pulse is generated for each photon detected and the signal is available at the BNC connector at the rear of the module. The signal should be terminated into 50 Ω. The photodiode is both thermoelectrically cooled and temperature controlled, ensuring stabilized performance despite ambient temperature changes. This detector has a jitter of 300-400 ps and their signals are collected by two QuTau. The QuTau is a time-to-digital converter that for each incoming event stores a 64 bit value of time arrival with a time bin size of 81 ps.

Chapter 5

Hyper-entangled photons Measurements and Stabilization

In the previous chapters we discuss the experimental setup and the production of hyperentangled photons pairs. In this one we'll explain how to perform measurements on the two entangled degrees of freedom, the issue of the experimental setup and their solutions, in particular the instability of the interferometers.

5.1 Polarization measurement

When dealing with polarized states, Jones arithmetic[20] is commonly used. Jones vectors are used to characterize a monochromatic plane wave that travels in the z direction. Let us consider the electric field

$$\mathcal{E}(z,t) = \Re\left\{A\exp\left[i\omega\left(t-\frac{z}{c}\right)\right]\right\} \tag{5.1}$$

where the complex envelope $A = A_x\hat{x}+A_y\hat{y}$ is a vector with complex components $A_x = a_x e^{i\varphi_x}$ and $A_y = a_y e^{i\varphi_y}$. The Jones vectors represent a way to express these quantities in form of a column matrix

$$J = \begin{bmatrix} A_x \\ A_y \end{bmatrix} \tag{5.2}$$

Since we are working at single photon, we don't care of the intensity value[1] so we express the Jones vector with normalized intensity. In the following table we provide the Jones vectors for some particular polarization states.

[1] If needed, we can obtain the intensity value by the number of photons recorded

Linear polarization in x ($\|H\rangle$): $\begin{pmatrix} 1 \\ 0 \end{pmatrix}$	Linear polarization at angle θ: $\begin{pmatrix} \cos\theta \\ \sin\theta \end{pmatrix}$
Right-circular polarization ($\|R\rangle$): $\frac{1}{\sqrt{2}}\begin{pmatrix} 1 \\ i \end{pmatrix}$	Left-circular polarization ($\|L\rangle$): $\frac{1}{\sqrt{2}}\begin{pmatrix} 1 \\ -i \end{pmatrix}$

Table 5.1: Jones vectors for linear polarized light and right and left-circular polarized light

In Jones vector we can express the Bell's states like:

$$\left|\Psi^{\pm}\right\rangle = \frac{1}{\sqrt{2}}\left(\begin{bmatrix} 1 \\ 0 \end{bmatrix}_A \begin{bmatrix} 0 \\ 1 \end{bmatrix}_B \pm \begin{bmatrix} 0 \\ 1 \end{bmatrix}_A \begin{bmatrix} 1 \\ 0 \end{bmatrix}_B\right) \quad . \tag{5.3}$$

Since we want to measure several kind of polarization states, polarization devices are needed to change the polarization. In a general approach, the new polarization state results by a weight superposition of the original one:

$$\begin{pmatrix} A_{2x} \\ A_{2y} \end{pmatrix} = \begin{pmatrix} T_{11} & T_{12} \\ T_{21} & T_{22} \end{pmatrix} \begin{pmatrix} A_{1x} \\ A_{1y} \end{pmatrix} \tag{5.4}$$

that can be easily written, calling J_1 and J_2 the input and output Jones vectors respectively, like

$$J_2 = T J_1. \tag{5.5}$$

The matrix T, called Jones matrix, describes a polarization device, where the vector J_1 and J_2 describe the input and output waves.

In our experiment, we need a device that can change any polarization state in a vertical polarization state, in fact a polarizing beam splitter (and in general any polarizer) lets pass only vertical polarization and reflects the horizontal one. To change the polarization state, wave retarder is usually used.

Wave retarders are birefringent plates with different refractive indices associated to different directions. Hence ordinary component of electric field will have greater group velocity than the extraordinary one. This implies that a phase difference between o and e components is generated inside the plate:

$$\Delta\varphi = \frac{2\pi}{\lambda}\left(n_o - n_e\right) L. \tag{5.6}$$

where n_o and n_e are the ordinary and extraordinary reflective index, λ is the wavelength of the beam and L is the length of the crystal. By varying the length of the crystal it's possible to introduce any phase value.

The following plates are of great importance:

- $\frac{\lambda}{4}$ wave plates where the coefficient $\frac{n_o - n_e}{\lambda} L$ is an odd multiple of $\frac{1}{4}$ so that the outcoming phase difference is $\frac{\pi}{2}$ less than a multiple of 2π. This kind of plates are used to transform circular polarization state in linear state and vice versa.

- $\frac{\lambda}{2}$ wave plates where the coefficient $\frac{n_o - n_e}{\lambda} L$ is an odd multiple of $\frac{1}{2}$ so that the outcoming phase difference is π less than a multiple of 2π. This kind of plates are used to rotate linear polarization state.

This information let us guess that these two polarization devices with a vertical optical axis can be represent by the following Jones matrices:

$$P_{\frac{\lambda}{4}} = \begin{pmatrix} 1 & 0 \\ 0 & -i \end{pmatrix} \tag{5.7}$$

$$P_{\frac{\lambda}{2}} = \begin{pmatrix} 1 & 0 \\ 0 & -1 \end{pmatrix} \tag{5.8}$$

and considering the rotation operator

$$R(\theta) = \begin{pmatrix} \cos\theta & -\sin\theta \\ \sin\theta & \cos\theta \end{pmatrix} \tag{5.9}$$

the general case becomes

$$P_{\frac{\lambda}{4}}(\theta) = R^{-1}(\theta) P_{\frac{\lambda}{4}} R(\theta) = \begin{pmatrix} \cos^2\theta - i\sin^2\theta & (1+i)\sin\theta\cos\theta \\ (1+i)\sin\theta\cos\theta & \sin^2\theta - i\cos^2\theta \end{pmatrix} \tag{5.10}$$

$$P_{\frac{\lambda}{2}}(\theta) = R^{-1}(\theta) P_{\frac{\lambda}{2}} R(\theta) = \begin{pmatrix} \cos 2\theta & \sin 2\theta \\ \sin 2\theta & -\cos 2\theta \end{pmatrix}. \tag{5.11}$$

As we've already said the polarizing beam splitter (PBS) is a device that transmits waves that have a vertical polarization and reflects the ones that have the orthogonal one. Therefore the vertical oriented PBS can be expressed as

$$P_V = \begin{pmatrix} 0 & 0 \\ 0 & 1 \end{pmatrix}. \tag{5.12}$$

For example we show what happens when we apply $\frac{\lambda}{2}$ wave plates on a general linear polarized light $\begin{pmatrix} \cos\alpha \\ \sin\alpha \end{pmatrix}$:

$$\begin{aligned} P_{\frac{\lambda}{2}}(\theta) \begin{pmatrix} \cos\alpha \\ \sin\alpha \end{pmatrix} &= \begin{pmatrix} \cos 2\theta & \sin 2\theta \\ \sin 2\theta & -\cos 2\theta \end{pmatrix} \begin{pmatrix} \cos\alpha \\ \sin\alpha \end{pmatrix} \\ &= \begin{pmatrix} \cos 2\theta\cos\alpha + \sin 2\theta\sin\alpha \\ \sin 2\theta\cos\alpha - \cos 2\theta\sin\alpha \end{pmatrix} \\ &= \begin{pmatrix} \cos(2\theta - \alpha) \\ \sin(2\theta - \alpha) \end{pmatrix} \end{aligned} \tag{5.13}$$

This means that a linear polarized light becomes a new linear polarized light with angle $2\theta - \alpha$. It's easy to understand that if we force $\theta = (\pi/2 + \alpha)/2$ we obtain

$$\begin{aligned} \begin{pmatrix} \cos(2\theta - \alpha) \\ \sin(2\theta - \alpha) \end{pmatrix} &= \begin{pmatrix} \cos\left(2\frac{\frac{\pi}{2}+\alpha}{2} - \alpha\right) \\ \sin\left(2\frac{\frac{\pi}{2}+\alpha}{2} - \alpha\right) \end{pmatrix} \\ &= \begin{pmatrix} \cos\left(\frac{\pi}{2} + \alpha - \alpha\right) \\ \sin\left(\frac{\pi}{2} + \alpha - \alpha\right) \end{pmatrix} \\ &= \begin{pmatrix} \cos\left(\frac{\pi}{2}\right) \\ \sin\left(\frac{\pi}{2}\right) \end{pmatrix} = \begin{pmatrix} 0 \\ 1 \end{pmatrix} \end{aligned} \tag{5.14}$$

So using a $\frac{\lambda}{2}$ wave plate we can transform any linear polarized light in a vertical polarized light.

Now let us see what happens when we apply $\frac{\lambda}{4}$ wave plates on a right circular polarized light

$$\begin{aligned} P_{\frac{\lambda}{4}}(\theta)\frac{1}{\sqrt{2}}\begin{pmatrix} 1 \\ i \end{pmatrix} &= \frac{1}{\sqrt{2}}\begin{pmatrix} \cos^2\theta - i\sin^2\theta & (1+i)\sin\theta\cos\theta \\ (1+i)\sin\theta\cos\theta & \sin^2\theta - i\cos^2\theta \end{pmatrix}\begin{pmatrix} 1 \\ i \end{pmatrix} \\ &= \frac{1}{\sqrt{2}}\begin{pmatrix} \cos^2\theta - i\sin^2\theta - (i-1)\sin\theta\cos\theta \\ (1+i)\sin\theta\cos\theta + i\sin^2\theta + \cos^2\theta \end{pmatrix} \\ &= \frac{1}{\sqrt{2}}\begin{pmatrix} \cos^2\theta - \sin\theta\cos\theta + i\left(\sin\theta\cos\theta - \sin^2\theta\right) \\ \sin\theta\cos\theta + \cos^2\theta + i\left(\sin^2\theta + \sin\theta\cos\theta\right) \end{pmatrix} \\ &= \begin{pmatrix} \sqrt{\frac{1}{2} - \cos\theta\sin\theta}\angle\theta \\ \sqrt{\frac{1}{2} + \cos\theta\sin\theta}\angle\theta \end{pmatrix} \end{aligned} \tag{5.15}$$

In this case we found that both the vector components have the same phase. This means that there is no global phase because one phase deletes the other one. Furthermore we can see that the square sum of the module of the Jones vector components is equal to 1. Using this info we can affirm that

$$\begin{pmatrix} \sqrt{\frac{1}{2} - \cos\theta\sin\theta} \\ \sqrt{\frac{1}{2} + \cos\theta\sin\theta} \end{pmatrix} = \begin{pmatrix} \cos\varphi \\ \sin\varphi \end{pmatrix} \tag{5.16}$$

Similar results can be found using left circular polarized light. As we've just seen using a $\frac{\lambda}{4}$ wave plate we can transform circular polarized light in linear polarized light. So using both $\frac{\lambda}{2}$ and $\frac{\lambda}{4}$ wave plates we can transform linear polarized light and circular polarized light in vertical polarized light that is selected by the PBS.

5.2 Time-bin measurement

In order to measure the time-bin entangled states we need two more interferometers similar to the one used to create the entangled state. When we try to perform a measure on the single detector the state described in formula 4.1 becomes

$$\begin{aligned} |\tau_A\rangle &= \frac{1}{\sqrt{2}}\left(|S\rangle + e^{i(\phi+\alpha)}|L\rangle\right) \\ |\tau_B\rangle &= \frac{1}{\sqrt{2}}\left(|S\rangle + e^{i(\phi+\beta)}|L\rangle\right) \end{aligned} \tag{5.17}$$

where $|S\rangle$ and $|L\rangle$ represent the short and long states, α and β represent respectively the phase induced by the path difference between long (D_i) and short

(d_i) arms:

$$\begin{aligned}\alpha &= 2\pi\frac{D_A - d_A}{\lambda}\\ \beta &= 2\pi\frac{D_B - d_B}{\lambda}\end{aligned} \tag{5.18}$$

where λ is the wavelength of the beam. From this we understand that the interferometers behave like a projection described by

$$P_\tau = \frac{1}{\sqrt{2}}\left(|S\rangle + e^{i\alpha}|L\rangle\right)\left(\langle S| + e^{-i\alpha}\langle L|\right) \tag{5.19}$$

where α is the phase induced by the path difference between long (D_i) and short (d_i) arms. As a result we found that the coincidences rate is

$$\begin{aligned}C(\alpha,\beta) &= \left|\frac{1}{2}\left(\langle S|_A + e^{-i\alpha}\langle L|_A\right)\left(\langle S|_B + e^{-i\beta}\langle L|_B\right)\frac{1}{\sqrt{2}}\left(|S\rangle_A|S\rangle_B + e^{i\phi}|L\rangle_A|L\rangle_B\right)\right|^2\\ &= \frac{1}{8}\left|\Big(\langle S|_A\langle S|_B + e^{-i\alpha}\langle L|_A\langle S|_B + e^{-i\beta}\langle S|_A\langle L|_B + e^{-i(\alpha+\beta)}\langle L|_A\langle L|_B\Big)\right.\\ &\quad\left.\left(|S\rangle_A|S\rangle_B + e^{i\phi}|L\rangle_A|L\rangle_B\right)\right|^2\\ &= \frac{1}{8}\left|\left(1 + e^{i(\phi-\alpha-\beta)}\right)\right|^2\\ &= \frac{1}{2}\cos^2\left(\frac{\phi-\alpha-\beta}{2}\right)\end{aligned} \tag{5.20}$$

It has to be noted that the formula 5.20 is similar to the polarization entanglement equation. This fact suggests that the time measurements can be performed as the polarization ones, where relative phases are obtained by varying long arms length.

Besides it is also possible to block the light beam passing through the long or the short arms of the interferometers. This operation is useful to project the time-bin entangled state in the $\frac{1}{\sqrt{2}}|S\rangle$ and $\frac{1}{\sqrt{2}}|L\rangle$ states that are needed to perform tomography measurement. To be noted that in this case we have to double the measurement time because the states that we are projecting are not normalized and this involves a difference of a factor 2 from the normalized one.

5.3 Interferometer stabilization

As we have seen in section 5.2 the time-bin coincidences rate depends on three phases value of the three interferometer. Every phases are determined by the path difference length between the long (D) and short (d) arms of the interferometers and by the wavelength λ of the beam, following the formula

$$\varphi = 2\pi\frac{D-d}{\lambda}. \tag{5.21}$$

Considering that:

1. an increase in temperature produces a thermal expansion and this affects the length difference of the interferometers arms;

2. the laser source, Mira-HP Coherent, has a small wavelength drift since it's a device with a tunable wavelength.

we can infer that the system is very unstable. In fact taking in account that the path difference between the long and small arms is about $30\,cm$ a variation of $1.8\,pm$ of the wavelength, leads to a phase shift of π. To solve these problems and

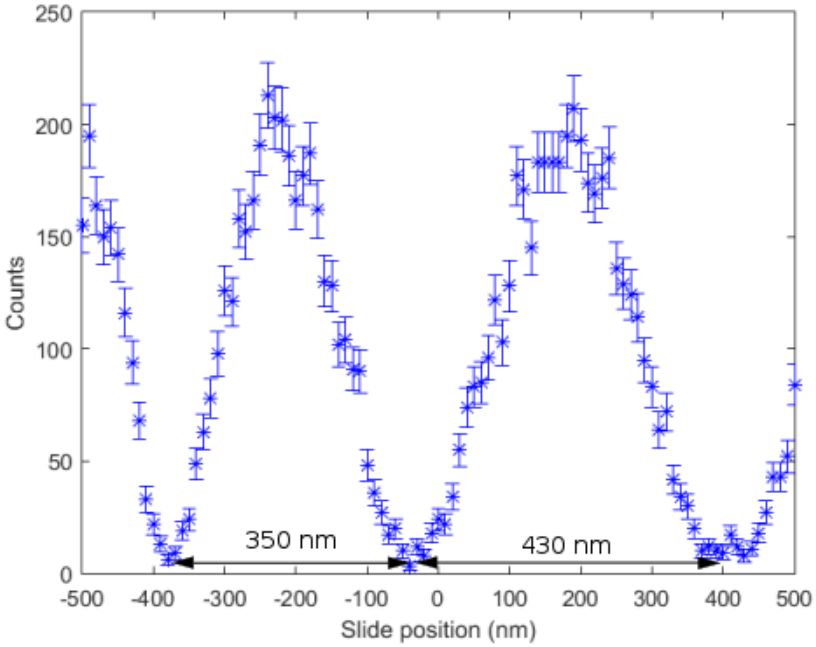

Figure 5.1: Here we report the interference pattern when moving one of the two slides regarding an acquisition time of about 5 seconds. It can be noted that the periods of the interference are different in two consecutive sinusoid (check the difference among the relative minimum). This is caused by the instability of the wavelength.

in particular the wavelength drift problem, a stabilization of the interferometers is needed. To calibrate the last interferometers, where the mirror on the long path is fixed on a nanometric slide controlled electrically, we use a small part of the original oscillator beam, which we call calibration light. This light, that is taken before SHG plate, is properly delayed in order to not overlap with the hyperentangled photons and it's added just after SHG plate. I. e., before the SPDC crystal there are two beams where one has double frequency of the other one. Following the path of the calibration light, after the pump interferometer

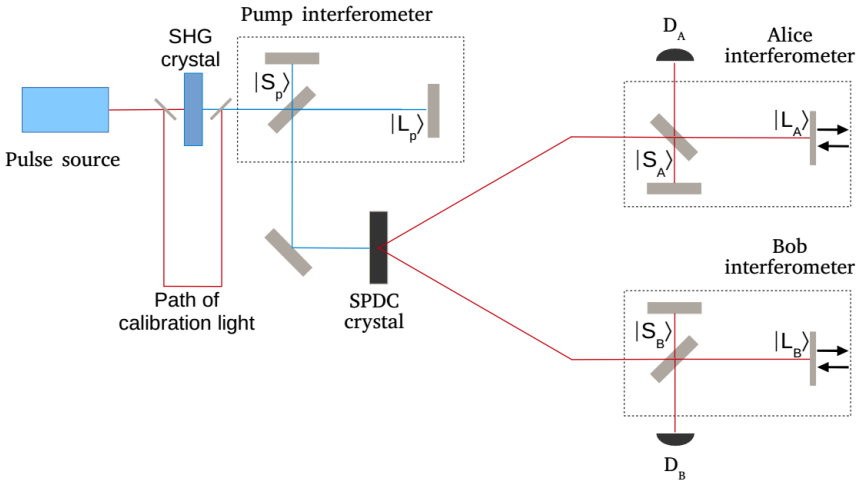

Figure 5.2: Conceptual scheme of stabilization

the light state is

$$|\Psi\rangle_p^C = \frac{1}{\sqrt{2}}\left(|S_p\rangle + e^{i\phi_p}|L_p\rangle\right) \tag{5.22}$$

where $|S\rangle_p$ and $|L\rangle_p$ represent respectively the long (with length D_p) and short (with length d_p) arms of the pump interferometer and $\phi_p = 2\pi\frac{D_p - d_p}{\lambda_{red}}$, $\lambda_{red} = 808\,nm$. After the SPDC crystal, the light splits in two beams, one follows Alice path, the other follows Bob path. If we look at the state that we get after Alice interferometer we obtain

$$|\Psi\rangle_A^C = \frac{1}{2}\left(|S_pS_A\rangle + e^{i\phi_p}|L_pS_A\rangle + e^{i\phi_A}|S_pL_A\rangle + e^{i(\phi_p+\phi_A)}|L_pL_A\rangle\right) \tag{5.23}$$

where ϕ_A is the phase shift induced by Alice interferometer. The photons that have chosen the short arms of both interferometers are represented by the state $|S_pS_A\rangle$. The photons that have chosen the long arm of the pump interferometer and the short arm of Alice interferometer are represented by the state $|L_pS_A\rangle$. The photons that have chosen the short arm of the pump interferometer and the long arm of Alice interferometer are represented by the state $|S_pL_A\rangle$. The photons that have chosen the long arms of both interferometers are represented by the state $|L_pL_A\rangle$. The events that we consider are those marked by $|L_pS_A\rangle$ and $|S_pL_A\rangle$ states that are indistinguishable, since they have the same travel time. By an easy manipulation of this subset of states we can write

$$e^{i\phi_p}|L_pS_A\rangle + e^{i\phi_A}|S_pL_A\rangle = |L_pS_A\rangle + e^{i(\phi_A-\phi_p)}|S_pL_A\rangle \tag{5.24}$$

that means that the counts rate is

$$N_A \propto \cos^2\frac{\phi_A - \phi_p}{2}. \tag{5.25}$$

This formula represent an interference.

Similar results are achieved considering the light path to Bob interferometer that leads to

$$N_B \propto \cos^2 \frac{\phi_B - \phi_p}{2}. \tag{5.26}$$

where N_B represent the counts rate and ϕ_B represent the phase shift induced by Bob interferometer.

Now let us observe what happens to the entangled light. At the end of the pump interferometer, we obtain a similar state of the calibration light:

$$|\Psi\rangle_p^e = \frac{1}{\sqrt{2}} \left(|S_p\rangle + e^{i\phi_e} |L_p\rangle \right). \tag{5.27}$$

In this case, contrary to the calibration light, we have a different phase shift due to the different wavelength, in fact we obtain

$$\phi_e = 2\pi \frac{D_p - d_p}{\lambda_{SHG}} = 2 \left(2\pi \frac{D_p - d_p}{\lambda_{red}} \right) = 2\phi_p, \; \lambda_{SHG} = \frac{\lambda_{red}}{2} = 404\, nm. \tag{5.28}$$

The complete state that we obtain after Alice and Bob interferometers is instead

$$\begin{aligned} |\Psi\rangle_{AB}^e = \frac{1}{2\sqrt{2}} \big(& |S_p S_A, S_p S_B\rangle + e^{i\phi_e} |L_p S_A, L_p S_B\rangle + e^{i\phi_A} |S_p L_A, S_p S_B\rangle \\ & + e^{i(\phi_e + \phi_A)} |L_p L_A, L_p S_B\rangle + e^{i\phi_B} |S_p S_A, S_p L_B\rangle + e^{i(\phi_e + \phi_B)} |L_p S_A, L_p L_B\rangle \\ & + e^{i(\phi_A + \phi_B)} |S_p L_A, S_p L_B\rangle + e^{i(\phi_e + \phi_A + \phi_B)} |L_p L_A, L_p L_B\rangle \big) \end{aligned} \tag{5.29}$$

where ϕ_A and ϕ_B is the phase shift induced by Alice and Bob interferometers. The events marked with the state $|S_p S_A, S_p S_B\rangle$ represent the photons that have chosen the short arms of all interferometers during they path. The events marked with the state $|L_p S_A, L_p S_B\rangle$ represent the photons that have chosen the long arm of the pump interferometer and the short arms of Alice and Bob interferometers. The events marked with the state $|S_p L_A, S_p S_B\rangle$ represent the photons that have chosen the short arms of the pump and Bob interferometers and the long arm of Alice interferometer.The events marked with the state $|L_p L_A, L_p S_B\rangle$ represent the photons that have chosen the long arms of the pump and Alice interferometers and the short arm of Bob interferometer. The events marked with the state $|S_p S_A, S_p L_B\rangle$ represent the photons that have chosen the short arms of the pump and Alice interferometers and the long arm of Bob interferometer.The events marked with the state $|L_p S_A, L_p L_B\rangle$ represent the photons that have chosen the long arms of the pump and Bob interferometers and the short arm of Alice interferometer. The events marked with the state $|S_p L_A, S_p L_B\rangle$ represent the photons that have chosen the short arm of the pump interferometer and the long arms of Alice and Bob interferometers. In the end the events marked with the state $|L_p L_A, L_p L_B\rangle$ represent the photons that have chosen the long arms of all interferometers. In this case the events that represent

the time-bin entangled state are $|S_pL_A, S_pL_B\rangle$ and $|L_pS_A, L_pS_B\rangle$. Considering only the events just mentioned we have the state

$$e^{i\phi_e}|L_pS_A, L_pS_B\rangle + e^{i(\phi_A+\phi_B)}|S_pL_A, S_pL_B\rangle = |L_pS_A, L_pS_B\rangle + e^{i(\phi_A+\phi_B-\phi_e)}|S_pL_A, S_pL_B\rangle . \tag{5.30}$$

So the counts rate is

$$N_C \propto \cos^2 \frac{\phi_A + \phi_B - \phi_e}{2} \tag{5.31}$$

that is equal to the formula 5.20. Calling $\phi_\alpha = (\phi_A - \phi_p)/2$ and $\phi_\beta = (\phi_B - \phi_p)/2$ and considering that $\phi_e = 2\phi_p$ we note that

$$\begin{aligned} \phi_\alpha + \phi_\beta &= \frac{\phi_A - \phi_p + \phi_B - \phi_p}{2} = \frac{\phi_A + \phi_B - 2\phi_p}{2} = \frac{\phi_A + \phi_B - \phi_e}{2} \\ N_C &\propto \cos^2 \frac{\phi_A + \phi_B - \phi_e}{2} = \cos^2(\phi_\alpha + \phi_\beta) \end{aligned} \tag{5.32}$$

Summarizing moving the linear actuators we can fix the counts rate of Alice and Bob interference (N_A and N_B), this process set the values of ϕ_α and ϕ_β which determines the total phase of the entangled state.

Thus the stabilization algorithm perform a rapid measurement (usually less than a second) and from this we calculate N_A and N_B values. Considering that the interference is a sinusoidal function, it's possible to move the linear actuators on Alice and Bob interferometers in order to stabilize the values of N_A and N_B. This algorithm has two big problems:

1. near the maximum and the minimum of interference, the sensibility of the Alice and Bob counts rate is almost null when changing the slide position;
2. near the maximum (minimum) it's difficult to realize if we are before or after the maximum (minimum).

To solve these problems we develop a new approach. The idea behind this new algorithm is the following:

1. We use all three peaks, generated by the calibration light (we call $Peak_1^C$ the peak generated by the events $|S_pS_{A(B)}\rangle$, $Peak_3^C$ the peak generated by the events $|L_pL_{A(B)}\rangle$ and $Peak_2^C$ the peak generated by the events $|S_pL_{A(B)}\rangle$ and $|L_pS_{A(B)}\rangle$). We define the parameter

$$R_{cal} = \frac{Peak_2^C}{Peak_1^C + Peak_3^C} \tag{5.33}$$

that is stable even if there is some power fluctuation in the laser pump. We use this parameter to select a point near the maximum value of the derivative of the interference function[2], which guarantees a high sensibility of the position of the linear actuator, correspondent to the selected phase, i. e., we look for the slide position that have $R_{cal} = 1$.

[2]The interference function is $I = I_1 + I_2 + 2|G|\sqrt{I_1 I_2}\cos\varphi$, where G is a parameter that weight the cross correlation between I_1 and I_2, φ it's the phase of G, and I_1 and I_2 represent the beams that are interfering. In our case I_1 and I_2 are $Peak_1^C$ and $Peak_3^C$ and I is $Peak_2^C$.

2. Knowing the dependence of the interference phase with the slide movement[3], we move the slide at the desire position.

3. At this point we perform a measurement of about 3 seconds.

4. We move back the slide and restart from point 1.

This algorithm is performed during any stabilized measure and using this we reached 99% of visibility of the time-bin entangled state (figure 5.10).

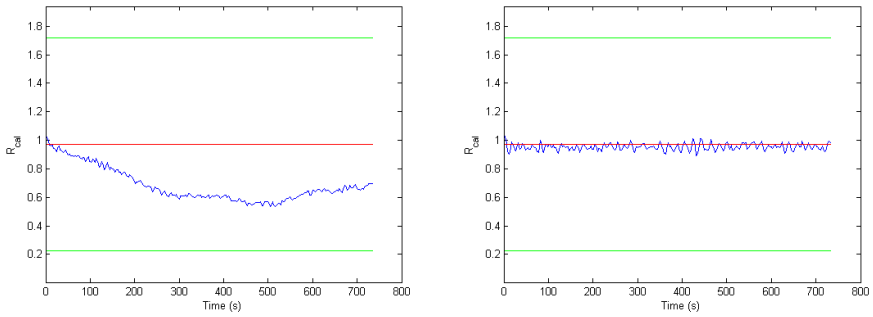

Figure 5.3: We can see how change the value of R_{cal} without the interferometer stabilization on the left and with the stabilization on the right.

5.4 Time synchronization

Before explaining how to synchronize two different measurements, we'll remember the measurement devices. To measure a polarization state, we use the $\lambda/2$ and $\lambda/4$ plates to project the wanted polarization on the polarizing beam splitter. To measure the time states we move the nanometric slides to change the interferometer phase or we block the light beam in one of the arms of the interferometers. After this, for both Alice and Bob we collect the outcoming photons with two Single Photon Avalanche photoDiodes (SPAD). For each revealed photon they send a TTL pulse that is registered on two Time to Digital Converter (TDC), QuTau, one for each SPAD, with a time unit of 81 ps (accuracy) that we call bin. To process our data we have to fix a time reference. To do so we take part of a pulsed signal outcoming the SHG crystal. This signal is detected by a photo-diode that produces a 76 MHz analog signal that is registered and decimated by an FPGA with a ratio of 1 to 15200. We call this, trigger signal. The trigger signal is registered on Alice QuTau and used to modulate a laser diode which emits light at 810 nm. This pulsed diode laser provides an optical link between Alice and Bob. After this Bob detects the light from a pulsed laser

[3]This can be deduced by recording $Peak_2^C$ while the correspondent slide is moving in a direction.

diode using a photo-diode. The photo-diode generates a square signal that is registered by Bob QuTau.

Therefore, Alice (Bob) QuTau will register:

- signals coming from photons on Alice (Bob) channel;
- trigger signals that provide a time reference.

Thus, Alice and Bob QuTau provide two arrays like

t_1^A	t_2^A	t_3^A	t_4^A	t_5^A	t_6^A	t_7^A	t_8^A	t_9^A	t_{10}^A	t_{11}^A	t_{12}^A	t_{13}^A	t_{14}^A	t_{15}^A	t_{16}^A
A	A	T	A	T	T	A	T	T	T	A	T	A	A	T	A

Table 5.2: Alice QuTau array. First row represents the time tag of the event registered in the second row

t_1^B	t_2^B	t_3^B	t_4^B	t_5^B	t_6^B	t_7^B	t_8^B	t_9^B	t_{10}^B	t_{11}^B	t_{12}^B	t_{13}^B	t_{14}^B	t_{15}^B	t_{16}^B
B	T	T	B	B	T	B	T	B	T	T	T	B	B	B	T

Table 5.3: Bob QuTau array. First row represents the time tag of the event registered in the second row

There are some problems related with the time arrivals on the TDCs.

1. A delay between t_1^B and t_1^A will be measured. It depends on the distance between Alice and Bob and their own electronics;
2. During the characteristic time of some seconds, which is the duration of a single measure, the TDCs will drift in a different way from each other.

The first problem is easily addressed by subtracting t_A^1 and t_B^1 to their own time tag. The real problem resides in how to understand if that event is registered by the same original impulse. To do so firstly we disable temporarily all the channels not related to the trigger signal. Then using a shutter, we interrupt the signal to Alice photo-diode. We reset both the QuTau arrays. At this point the shutter opens rapidly and the same pulse will be registered by the parties. We enable all the channels.

The second problem is more complex and requires some analysis to solve it. The presence of a drift between the TDCs means that

$$t_{i+m}^A - t_i^A \neq t_{i+n}^B - t_i^B \tag{5.34}$$

where t_i^A (t_i^B) and t_{i+m}^A (t_{i+n}^B) represent the triggers, produced by the same event, in Alice (Bob) arrays. This happens because the clocks in the two different devices work slightly different. However in a few seconds the TDCs can registered a time difference of tenths seconds. Considering that the coincidence

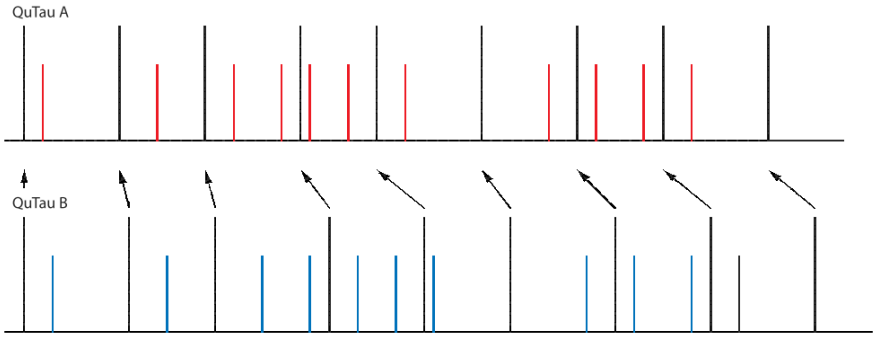

Figure 5.4: Here we can observe an example of Alice QuTau (QuTau A) and Bob QuTau (QuTau B). The Black events, represent a trigger signals, the blue and red events represent a photon signals. It's easily to note that Alice and Bob have the correspondent trigger signal at different time.

windows is of few nanoseconds, this problem must be solved to correlate the photons. The algorithm used to do so is the following

$$t_i^B - t_{tr_1}^B \rightarrow \left(t_i^B - t_{tr_1}^B\right) \frac{t_{tr_2}^A - t_{tr_1}^A}{t_{tr_2}^B - t_{tr_1}^B} \tag{5.35}$$

where $t_{tr_2}^A$, $t_{tr_1}^A$ are two consecutive trigger on the Alice arrays matching the trigger on Bob $t_{tr_2}^B$, $t_{tr_1}^B$. Furthermore t_i^B must be between $t_{tr_2}^B \, and \, t_{tr_1}^B$.

Practically the main idea is to use the trigger to divide the two main arrays in several small arrays, then to use the formula 5.35 to correct the drift between Alice and Bob.

Since these procedures have to be done during the stabilization of the interferometers, continuous measurements can not be preformed. This is due to the stabilization algorithm of the interferometers that require separate measurements. To solve this problem we use a dynamic library that works in parallel with the measurement program. This library continuously downloads the QuTau events of both Alice and Bob and works as follow:

1. Every few milliseconds the library downloads the data array from QuTau and retrieves two rows

2. It's checked if in the downloaded array any trigger event is missing .[4] If true a trigger event it's added with an estimated time tag. This can be done remembering that the trigger events have a fixed time difference, this information can be used to check if there is some missing event and to estimate the time of the missing event.

[4]If two events have the same time tag, the QuTau saves only the first one and discards the other one.

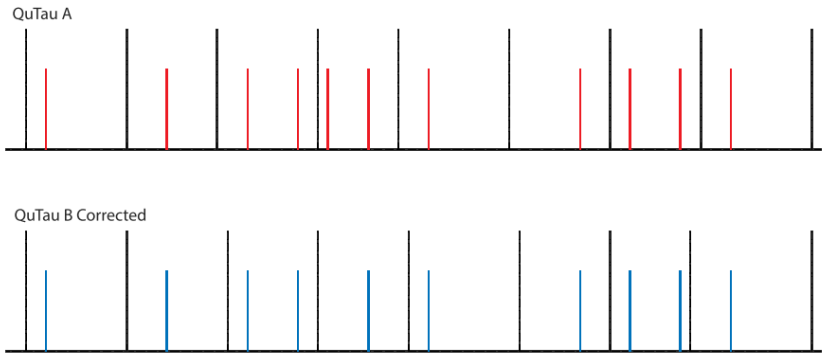

Figure 5.5: Here we can observe an example of Alice QuTau (QuTau A) and Bob QuTau (QuTau B) after the correction with formula 5.35. The Black events, represent a trigger signals, the blue and red events represent a photon signals. As a consequence of the correction, now we see that Alice and Bob signals happen at the same time.

3. A third row is added by the library. If an event is a trigger event then the third row is filled with the corresponding number of triggers registered from the first pulse registered. In all the other case the third row is filled with the time difference between the last trigger registered and the correspondent event and a module operation is applied to compensate the pulse decimation.

4. This new array is appended to a circular array in the dynamic library with a buffer of 1 million of events. Then the algorithm is repeated from the point 1.

This circular array can be downloaded by an external program at any time. It's particularly useful because after the first time synchronization, using the third row it's possible to stay synchronized even if not continuous measurements are performed. Furthermore this is useful to select only the common events between the Alice and Bob data that are the events between the same triggers numbers.

5.5 Calculation of Coincidences

After the synchronization problem is solved, we must find a standard to consider if two events, one from Alice and one from Bob, are due to entangled photons. To do this we fix a coincidences window, and check if both the event of Alice and Bob are inside. Thanks to the trigger signal, that is directly connected to the laser pulse and thus to the generation of entangled photons pair, we can refer the

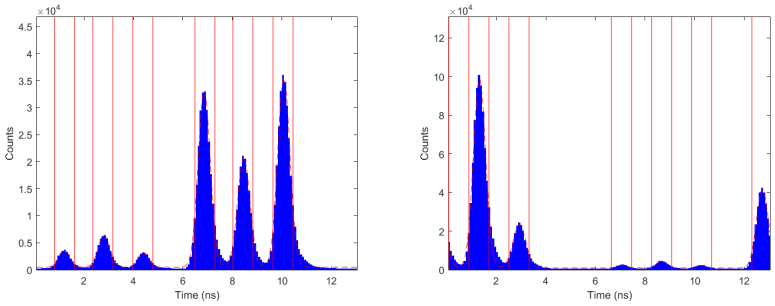

Figure 5.6: Histograms of time arrivals. We observe six peaks corresponding to the different paths along the pump interferometer and the measurement interferometer for the entangled and calibration light. We report the data with a window of 13 ns for the module operation. This is because the original signal was a 76 MHz pulsed one. It's evident that Alice (on the left) and Bob (in the right) have a different delay. This is corrected via software in order to find the coincidences.

photon time arrival to trigger time and apply a module operation to compensate the pulse decimation.[5] After this it becomes easy to distinguish what path the photons choose. We can note in figure 5.6 that for each channel there are a total of six peaks. If we observe more accurately we note that in reality we can distinguish two sets of three peaks per channel. The more intense set is due to the calibration light. Starting from the left, in this set, the first peak that we meet is due to the calibration photons that have selected the short arms in both the interferometers. Likewise, the third peak represents the photons that have selected the long arms in both the interferometers. We can also note that the middle peak, that is due to the calibration photons that have chosen the long arms in one of the interferometer and the short arm in the other, its intensity is different respect to the sum of the other two peaks, that means that there is interference as expected. In the same way we can distinguish the three peaks of the other set, that represent the entangled photons. We note in this case that the intensity of the middle peak is exactly the sum of the interference of the other two peaks. Observing Alice channel and Bob channel we can find a delay between the correspondent peaks. This it's due to the setup and the electronic devices. It remains fixed until the setup is unchanged.

Up to now we have observed the single events of Alice and Bob channels separately. To be able to distinguish entangled photons we need to observe the coincidences between these channels. Now we have to look at the subset of singles in which entangled photons could be found. It is important to remember that the entanglement is characterized by indistinguishable states. We can see in figure 5.7 , that the entangled photons are the black circles. In fact regarding

[5]This is already done by the dynamic library developed to perform the time synchronization.

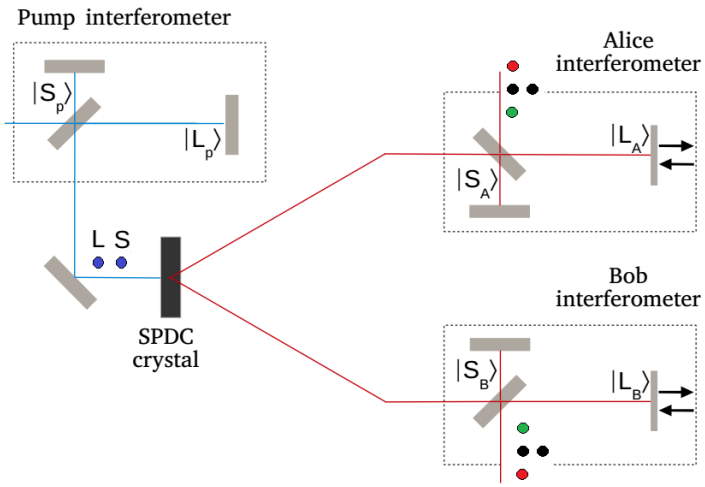

Figure 5.7: The pump photons run through the long or short path of the interferometers. This means that the entangled pairs could be generated in two different moments, so we observe two dots labeled as S and L. In the Alice and Bob interferometers, the photons can choose the long or short path. The entanglement is related with those photons for which we cannot know when they were generated, that are the black circled pairs. About the red pair we are certain that the pump photon chose the short path and that they were generated before. For the green pair we are certain that the pump photon chose the long path. In these case no superposition is present and as a consequence the photons are not entangled.

these photons we can not say which of the correspondent pump photons have taken the short or the long arms and so we don't know when they were generated. Because of these indistinguishable possibilities, we have the time-bin entangled pair.

$$|\tau_A\rangle = \frac{1}{\sqrt{2}}\left(|S\rangle_A |S\rangle_B + e^{i(\phi)} |L\rangle_A |L\rangle_B\right) \tag{5.36}$$

Using thresholds (red line in figure 5.6) we can select only the singles in the middle peak. We do this because no time-bin entangled photons can be found on the other peaks. Wides is the selection of the thresholds, the greater is the number of events obtained. However, this increases the ratio of accidents compared to the total events. So we need to balance these two behaviors. Because of conservation laws, the entangled photons should be generated at the same time. All pairs that will be found within a time window will be considered entangled photons. Even in this case we can find a delay between Alice and Bob events. This it's due to the setup and the electronics devices, so it remains fixed until the setup is unchanged and thanks to this property it can be easily found. In figure 5.8 we have an example of what we obtain.

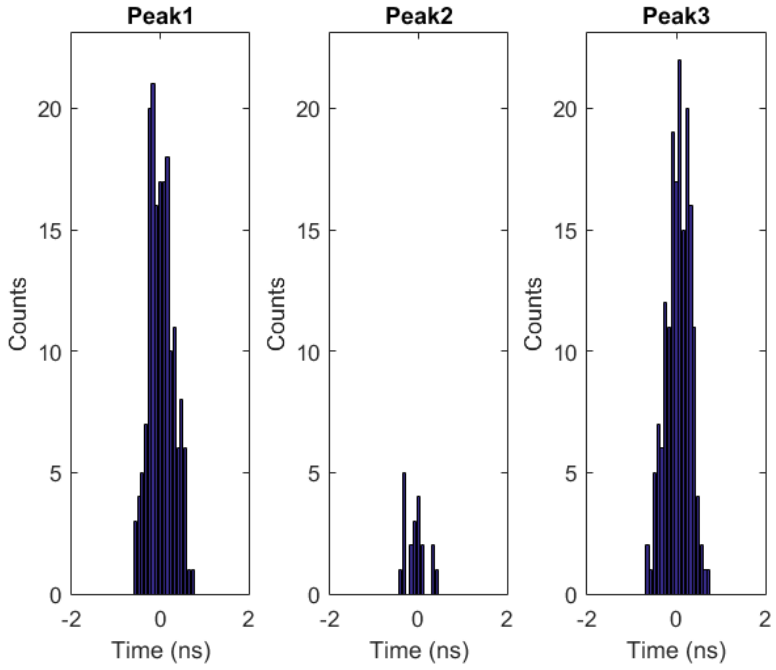

Figure 5.8: Histograms of the coincidences. We observe three peaks corresponding to the different path along the pump interferometer and the measurement interferometers. Starting from left we have the events correspondent to the state $|S_p S_{A,B}\rangle$, $\frac{1}{\sqrt{2}}\left(|L_p S_{A,B}\rangle + e^{i\phi} |S_p L_{A,B}\rangle\right)$, $|L_p L_{A,B}\rangle$. Peak1 and Peak3 are obviously separable states. Peak2 represent the time-bin entangled photons pair.

We will use this method to determine the counts of time-bin entangled photons for all the data we will acquire. We now observe that there could be also different situations from that described above. When performing a quantum tomography, for example, we will project a single photon on the state $|L\rangle$. Obviously no single photon will be found in the Peak1. None of the less, the counts found in Peak2 represent the coincidences of time-bin entangled photons.

Time-bin interference condition

To be able to find time-bin entangled events, some important conditions must be met.

$$\begin{cases} D & = D_p - d_p \gg l_{coh} \\ D_L & = |(D_A - d_A) - (D_B - d_B)| < l_{coh} \\ D_{L_1} & = \left|\left(D_{A(B)} - d_{A(B)}\right) - (D_p - d_p)\right| < l_{coh} \end{cases} \tag{5.37}$$

Here $D_i \, and \, d_i \, (i = p, \, A, \, B)$ respectively represent the length of long and short arms for the pump, Alice and Bob interferometers. l_{coh} represents the coherence length of the pulsed laser beam. For pulsed sources, the coherence length derives by the coherence time that is ultimately associated to single pulse duration. So the first condition is intended to guarantee that no single photon interference might happen. This is immediately verified because D is about 30 cm and the coherence time is around $250 \, fs$ that corresponds to a coherence length of about $75 \, \mu m$. The third condition can be verified by checking that moving the slides we create an interference pattern. If this pattern is centered around the zero value for each slide we can say that the third condition is met. The second condition puts some limits on the length difference between Alice and Bob interferometers long arms. Alternately moving Alice and Bob interferometers we found that when D_L and D_{L_1} tend to 0, the interference pattern grows up. To do so we moved one of the two slides with $3 \, \mu m$ step letting the second one in a fixed position. In this way we were able to plot an interference pattern such that in figure 5.1. In this figure we observe a growing interference around the zero value. Moreover we are able to estimate, even if not precisely, the coherence length for the photons. Thanks to this measure it is possible to estimate and improve the visibility of the state, defined as

$$\nu = \frac{C_{max} - C_{min}}{C_{max} + C_{min}} \tag{5.38}$$

where C_{max} and C_{min} label the maximum and minimum value of the fit for the interference pattern.

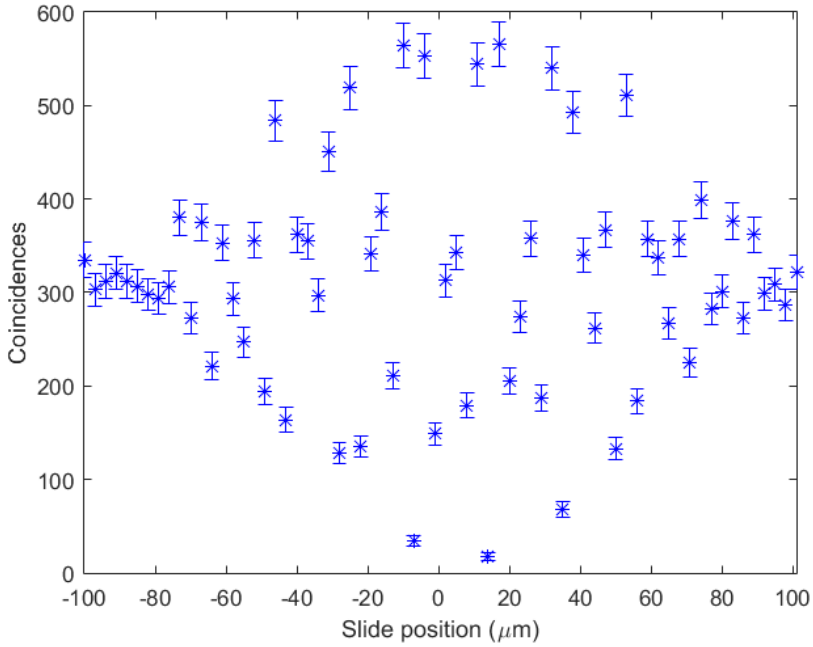

Figure 5.9: Interference pattern when moving one of the slide by a step of $3\,\mu m$.

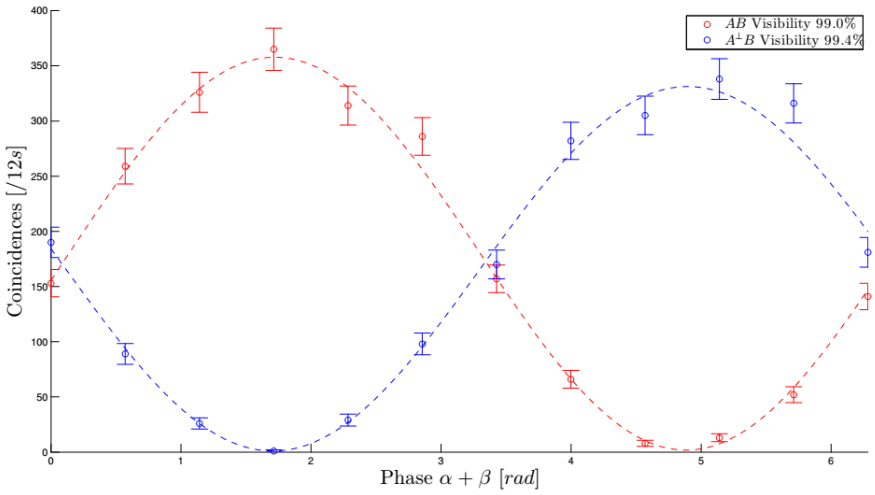

Figure 5.10: Visibility using stabilization algorithm.

5.6 Quantum Tomography Measure

Quantum tomography or quantum state tomography is the process of reconstructing the quantum state for a source of quantum systems by measurements of the systems coming from the source. Since we are working with qubits, that is a two-level system, it is more convenient to represent the quantum state as density matrix.

Expected Quantum State

Thanks to the previous sub-section we have explained what is a density matrix and how to use it. Then in this subsection we present the expected value.

In our experiment we get a polarization entangled state like

$$|\Psi\rangle = \frac{1}{\sqrt{2}}\left(|HV\rangle - |VH\rangle\right) \tag{5.39}$$

and a time-bin entangled state

$$|\Psi\rangle = \frac{1}{\sqrt{2}}\left(|SS\rangle - |LL\rangle\right) \tag{5.40}$$

In order to obtain the correspondent density matrix we apply formula 1.18 and we obtain

$$\begin{aligned}\hat{\rho}_P &= |\Psi\rangle\langle\Psi| \\ &= \frac{1}{2}\left(|HV\rangle - |VH\rangle\right)\left(\langle HV| - \langle VH|\right) \\ &= \frac{1}{2}\left(|HV\rangle\langle HV| - |VH\rangle\langle HV| - |HV\rangle\langle VH| + |VH\rangle\langle VH|\right)\end{aligned} \tag{5.41}$$

that can be expressed like

$$\hat{\rho}_P = \frac{1}{2}\begin{pmatrix} 0 & 0 & 0 & 0 \\ 0 & 1 & -1 & 0 \\ 0 & -1 & 1 & 0 \\ 0 & 0 & 0 & 0 \end{pmatrix}. \tag{5.42}$$

Regarding the time-bin entangled state we obtain

$$\begin{aligned}\hat{\rho}_P &= |\tau\rangle\langle\tau| \\ &= \frac{1}{2}\left(|SS\rangle - |LL\rangle\right)\left(\langle SS| - \langle LL|\right) \\ &= \frac{1}{2}\left(|SS\rangle\langle SS| - |SS\rangle\langle LL| - |LL\rangle\langle SS| + |LL\rangle\langle LL|\right)\end{aligned} \tag{5.43}$$

that, written in matrix form, becomes

$$\hat{\rho}_P = \frac{1}{2}\begin{pmatrix} 1 & 0 & 0 & -1 \\ 0 & 0 & 0 & 0 \\ 0 & 0 & 0 & 0 \\ -1 & 0 & 0 & 1 \end{pmatrix}. \tag{5.44}$$

Quantum Tomography

Finally we explain how quantum tomography works. To perform this measure we follow the paper presented in 2001 by Kwiat et al. [21].

We begin by explaining how to perform a single qubit tomography (no entangled state). The first of such experimental techniques for determining the state of a quantum system was devised by George Stokes in 1852. He defined a set of measurement that allows an experimenter to determine uniquely the polarization state of a light beam. Now these intensity measures are called Stokes parameters. They consist of:

1. measurement performed with a device which transmits half of the incident beam, regardless of its polarization;
2. measurement with a polarizer that transmits only horizontally polarized light;
3. measurement with a polarizer that transmits only light polarized at 45° to the horizontal;
4. measurement with a polarizer that transmits only right-circularly polarized light.

Calling N the complete rate of event regardless of their polarization, this four measurements correspond to

$$\begin{aligned} n_0 &= \frac{N}{2}\left(\langle H|\hat{\rho}|H\rangle + \langle V|\hat{\rho}|V\rangle\right) = \frac{N}{2}\left(\langle R|\hat{\rho}|R\rangle + \langle L|\hat{\rho}|L\rangle\right) \\ n_1 &= N\langle H|\hat{\rho}|H\rangle = \frac{N}{2}\left(\langle R|\hat{\rho}|R\rangle + \langle L|\hat{\rho}|L\rangle + \langle R|\hat{\rho}|L\rangle + \langle L|\hat{\rho}|R\rangle\right) \\ n_2 &= N\langle A|\hat{\rho}|A\rangle = \frac{N}{2}\left(\langle R|\hat{\rho}|R\rangle + \langle L|\hat{\rho}|L\rangle + i\langle R|\hat{\rho}|L\rangle - i\langle L|\hat{\rho}|R\rangle\right) \\ n_3 &= N\langle R|\hat{\rho}|R\rangle \end{aligned} \tag{5.45}$$

where $|H\rangle$, $|V\rangle$, $|A\rangle = 1/\sqrt{2}\left(|H\rangle - |V\rangle\right)$, $|R\rangle = 1/\sqrt{2}\left(|H\rangle - i|V\rangle\right)$ are the ket representation of the linear horizontal, linear vertical, linear diagonal (45°) and right-circular polarization. By this we calculate the Stokes parameters that completely characterize polarization state of the light

$$\begin{aligned} S_0 &\equiv 2n_0 = N\left(\langle R|\hat{\rho}|R\rangle + \langle L|\hat{\rho}|L\rangle\right) \\ S_1 &\equiv 2\left(n_1 - n_0\right) = N\left(\langle R|\hat{\rho}|L\rangle + \langle L|\hat{\rho}|R\rangle\right) \\ S_2 &\equiv 2\left(n_2 - n_0\right) = Ni\left(\langle R|\hat{\rho}|L\rangle + \langle L|\hat{\rho}|R\rangle\right) \\ S_3 &\equiv 2\left(n_3 - n_0\right) = N\left(\langle R|\hat{\rho}|R\rangle - \langle L|\hat{\rho}|L\rangle\right). \end{aligned} \tag{5.46}$$

So we can express the density matrix as

$$\hat{\rho} = \frac{1}{2}\sum_{i=0}^{3}\frac{S_i}{S_0}\hat{\sigma}_i \tag{5.47}$$

where $\hat{\sigma}_i$ represent the Pauli spin operator ($\hat{\sigma}_0 = |R\rangle\langle R| + |L\rangle\langle L|$, $\hat{\sigma}_1 = |R\rangle\langle L| + |L\rangle\langle R|$, $\hat{\sigma}_2 = i(|L\rangle\langle R| - |R\rangle\langle L|)$,$\hat{\sigma}_3 = |R\rangle\langle R| - |L\rangle\langle L|$).

When we want to measure a multiple qubit tomography, the generalization of the Stokes parameter can be helpful. However, one should be aware that single photons can be described in a purely classical manner, and the density matrix can be related to the purely classical concept of the coherency matrix. Instead multiple photons have the possibility of non-classical correlations occurring such as entanglement. The generalization at n-qubit state is characterized by a density matrix which may be written as

$$\hat{\rho} = \frac{1}{2^n} \sum_{i_1,i_2,\ldots,i_n=0}^{3} \frac{S_{i_1,i_2,\ldots,i_n}}{S_{0,0,\ldots,0}} \hat{\sigma}_{i_1} \otimes \hat{\sigma}_{i_2} \otimes \ldots \otimes \hat{\sigma}_{i_n} \tag{5.48}$$

where the 4^n parameters ($S_{i_1,i_2,\ldots,i_n}$) are real numbers and represent the numbers of measure that are needed to fully characterize the state. However, there is one important drawback to this method, in that the recovered state might not correspond to a physical state because of experimental noise. For example, density matrices for any quantum state must be Hermitian, positive semi-definite matrices with unitary trace. The tomographically measured matrices often fails to be positive semi-definite. A way to solve this problem is "maximum likelihood" tomographic.

Maximum likelihood method

The main idea behind the Maximum likelihood method is:

1. Generate an explicitly ''physical'' density matrix, i.e., a matrix that has the three important properties of normalization, Hermiticity, and positivity. This matrix will be a function of 16 real variables and will be denoted

$$\hat{\rho}_L(t_1, t_2, \ldots, t_{16}) \tag{5.49}$$

.

2. Create a "likelihood function" which quantifies how good the density matrix $\hat{\rho}_L(t_1, t_2, \ldots, t_{16})$ is in relation to the experimental data. This function will be denoted

$$\mathcal{L}(t_1, t_2, \ldots, t_{16}; n_1, n_2, \ldots, n_{16}) \tag{5.50}$$

3. Find the set of variable, denoted $\left\{t_1^{opt}, t_2^{opt}, \ldots, t_{16}^{opt}\right\}$, that maximizes the likelihood function. The best estimate for the density matrix is then

$$\hat{\rho}_L(t_1^{opt}, t_2^{opt}, \ldots, t_{16}^{opt}) \tag{5.51}$$

A matrix that can be written $\hat{G} = \hat{T}^\dagger \hat{T}$ it's non negative. This is easily explained in the following equality

$$\langle\psi|\hat{G}|\psi\rangle = \langle\psi|\hat{T}^\dagger\hat{T}|\psi\rangle = \langle\psi'|\psi'\rangle \geq 0 \tag{5.52}$$

where we have defined $|\psi'\rangle = \hat{T}|\psi\rangle$. Furthermore the matrix is also Hermitian, in fact

$$\left(\hat{T}^\dagger\hat{T}\right)^\dagger = \hat{T}^\dagger\left(\hat{T}^\dagger\right)^\dagger = \hat{T}^\dagger\hat{T} \tag{5.53}$$

To ensure normalization, we can simply divide the matrix by the trace obtaining

$$\hat{g} = \frac{\hat{T}^\dagger\hat{T}}{tr(\hat{T}^\dagger\hat{T})}. \tag{5.54}$$

This matrix has all three of the mathematical properties required for density matrices. Regarding an entangled states, that is a two qubits system, we need a 4×4 density matrix with 16 entries. It's convenient to choose a tridiagonal form for $\hat{T}$, since it will be useful to invert relation5.54.

$$\hat{T} = \begin{pmatrix} t_1 & 0 & 0 & 0 \\ t_5 + it_6 & t_2 & 0 & 0 \\ t_{11} + it_{12} & t_7 + it_8 & t_3 & 0 \\ t_{15} + it_{16} & t_{13} + it_{14} & t_9 + it_{10} & t_4 \end{pmatrix} \tag{5.55}$$

So the ''physical'' density matrix is

$$\hat{\rho}_L = \frac{\hat{T}^\dagger\hat{T}}{tr(\hat{T}^\dagger\hat{T})}. \tag{5.56}$$

Regarding the likelihood function, we suppose that the noise on the parameter has a Gaussian probability, where the standard error is approximately the square root of the real value. For a physical density matrix the number of count expected for the νth measurement is

$$\bar{n}_\nu(t_1, t_2, \ldots, t_{16}) = N\langle\psi_\nu|\hat{\rho}_L(t_1, t_2, \ldots, t_{16})|\psi_\nu\rangle \tag{5.57}$$

Thus the likelihood function is

$$P(t_1, t_2, \ldots, t_{16}; n_1, n_2, \ldots, n_{16}) = \frac{1}{N_{norm}} \prod_{\nu=1}^{16} \exp\left[\frac{\left(N\langle\psi_\nu|\hat{\rho}_L(t_1, t_2, \ldots, t_{16})|\psi_\nu\rangle - n_\nu\right)^2}{N\langle\psi_\nu|\hat{\rho}_L(t_1, t_2, \ldots, t_{16})|\psi_\nu\rangle}\right] \tag{5.58}$$

However it is easier to maximize its logarithm. Then in order to find the optimal parameters we minimize the following function

$$\mathcal{L}(t_1, t_2, \ldots, t_{16}; n_1, n_2, \ldots, n_{16}) = \sum_{\nu=1}^{16} \frac{\left(N\langle\psi_\nu|\hat{\rho}_L(t_1, t_2, \ldots, t_{16})|\psi_\nu\rangle - n_\nu\right)^2}{N\langle\psi_\nu|\hat{\rho}_L(t_1, t_2, \ldots, t_{16})|\psi_\nu\rangle} \tag{5.59}$$

A convenient set of measure is the following one:

ν	Mode 1	Mode 2
1	$\|H\rangle$	$\|H\rangle$
2	$\|H\rangle$	$\|V\rangle$
3	$\|V\rangle$	$\|V\rangle$
4	$\|V\rangle$	$\|H\rangle$
5	$\|R\rangle$	$\|H\rangle$
6	$\|R\rangle$	$\|V\rangle$
7	$\|D\rangle$	$\|V\rangle$
8	$\|D\rangle$	$\|H\rangle$
9	$\|D\rangle$	$\|R\rangle$
10	$\|D\rangle$	$\|D\rangle$
11	$\|R\rangle$	$\|D\rangle$
12	$\|H\rangle$	$\|D\rangle$
13	$\|V\rangle$	$\|D\rangle$
14	$\|V\rangle$	$\|L\rangle$
15	$\|H\rangle$	$\|L\rangle$
16	$\|R\rangle$	$\|L\rangle$

Where $|D\rangle = \frac{1}{\sqrt{2}}(|H\rangle + |V\rangle)$, $|L\rangle = \frac{1}{\sqrt{2}}(|H\rangle + i|V\rangle)$ and $|R\rangle = \frac{1}{\sqrt{2}}(|H\rangle - i|V\rangle)$. To be noted that with this set of measure $N = \sum_{\nu=1}^{4} n_\nu$.

Chapter 6

Experimental Results

In this section we report the results obtained in our experiment. We show that we can obtain a Bell inequality violation using polarization and time-bin degrees of freedom separately. Then we show, for the first time, that we can obtain violation of "chained" bell inequality a 6, 8, 10 parameters, proving that a local realist model with long realist delays can not describe the physical results. Finally, we present a time-bin and polarization entanglement quantum state tomography of hyperentangled photons using a free space channel, that it had never been done before.

6.1 Bell Measurement

These measurements were carried out following what we introduced in section 1.3. In order to find

$$S(\alpha, \beta, \alpha', \beta') = E(\alpha, \beta) - E(\alpha, \beta') + E(\alpha', \beta) + E(\alpha', \beta') \tag{6.1}$$

we need to measure

$$E(\alpha, \beta) = \frac{C(\alpha, \beta) - C(\alpha_\perp, \beta) - C(\alpha, \beta_\perp) + C(\alpha_\perp, \beta_\perp)}{C(\alpha, \beta) + C(\alpha_\perp, \beta) + C(\alpha, \beta_\perp) + C(\alpha_\perp, \beta_\perp)} \tag{6.2}$$

Normally, devices which are meant for these measurements are composed of a total of four detectors, two detectors for Alice and two for Bob. For example when we deal with polarization entangled states, one of detector receives the light transmitted by the PBS and the other receives the light reflected by the PBS. This allows to measure also the orthogonal state. Instead if we want to measure time-bin entangled states, Mach-Zehnder interferometers are used in place of those of Michelson, allowing to have also the orthogonal state likewise for the polarization one.

But our devices is composed only of two detectors, so to circumvent the problem we need to perform four measurements instead of one, one measurement for each $C(\vec{a}, \vec{b})$ in $E(\vec{a}, \vec{b})$.

The angles used to perform these measurements are the following (together with orthogonal angles needed to carry out the measures of the orthogonal state)

α	$\frac{\pi}{2}$	$\alpha_\perp$	0
β	$\frac{\pi}{8}\pi$	$\beta_\perp$	$\frac{5}{8}\pi$
α'	$\frac{3}{4}\pi$	$\alpha'_\perp$	$\frac{\pi}{4}$
β'	$\frac{3}{8}\pi$	$\beta'_\perp$	$\frac{7}{8}\pi$

The formula of the error propagation for $S(\alpha, \beta, \alpha', \beta')$ and $E(\alpha, \beta)$ are:

$$\begin{aligned}\sigma_{E(\alpha,\beta)} = \Bigg[&\left(\frac{\partial E(\alpha,\beta)}{\partial C(\alpha,\beta)}\right)^2 \sigma^2_{C(\alpha,\beta)} + \left(\frac{\partial E(\alpha,\beta)}{\partial C(\alpha_\perp,\beta)}\right)^2 \sigma^2_{C(\alpha_\perp,\beta)} \\ &+ \left(\frac{\partial E(\alpha,\beta)}{\partial C(\alpha,\beta_\perp)}\right)^2 \sigma^2_{C(\alpha,\beta_\perp)} + \left(\frac{\partial E(\alpha,\beta)}{\partial C(\alpha_\perp,\beta_\perp)}\right)^2 \sigma^2_{C(\alpha_\perp,\beta_\perp)} \Bigg]^{\frac{1}{2}}\end{aligned} \tag{6.3}$$

where

$$\frac{\partial E(\alpha,\beta)}{\partial C(\alpha,\beta)} = \frac{\partial E(\alpha,\beta)}{\partial C(\alpha_\perp,\beta_\perp)} = \frac{2C(\alpha_\perp,\beta) + 2C(\alpha,\beta_\perp)}{\left(C(\alpha,\beta) + C(\alpha_\perp,\beta) + C(\alpha,\beta_\perp) + C(\alpha_\perp,\beta_\perp)\right)^2} \tag{6.4}$$

$$\frac{\partial E(\alpha,\beta)}{\partial C(\alpha_\perp,\beta)} = \frac{\partial E(\alpha,\beta)}{\partial C(\alpha,\beta_\perp)} = \frac{-2C(\alpha,\beta) - 2C(\alpha_\perp,\beta_\perp)}{\left(C(\alpha,\beta) + C(\alpha_\perp,\beta) + C(\alpha,\beta_\perp) + C(\alpha_\perp,\beta_\perp)\right)^2} \tag{6.5}$$

and

$$\begin{aligned}\sigma_{S(\alpha,\beta,\alpha',\beta')} &= \Bigg[\left(\frac{\partial S(\alpha,\beta,\alpha',\beta')}{\partial E(\alpha,\beta)}\right)^2 \sigma^2_{E(\alpha,\beta)} + \left(\frac{\partial S(\alpha,\beta,\alpha',\beta')}{\partial E(\alpha',\beta)}\right)^2 \sigma^2_{E(\alpha',\beta)} \\ &\quad + \left(\frac{\partial S(\alpha,\beta,\alpha',\beta')}{\partial E(\alpha,\beta')}\right)^2 \sigma^2_{E(\alpha,\beta')} + \left(\frac{\partial S(\alpha,\beta,\alpha',\beta')}{\partial E(\alpha',\beta')}\right)^2 \sigma^2_{E(\alpha',\beta')} \Bigg]^{\frac{1}{2}} \\ &= \sqrt{\sigma^2_{E(\alpha,\beta)} + \sigma^2_{E(\alpha',\beta)} + \sigma^2_{E(\alpha,\beta')} + \sigma^2_{E(\alpha',\beta')}}\end{aligned} \tag{6.6}$$

Polarization

The polarization measurement has been performed without using the interferometers stabilization algorithms and with the light path of the long arm of the Alice and Bob interferometers blocked in order to avoid time-bin interference. The counts have been calculated using all two peaks that represent the entangled photons since we are interested in the polarization entangled photons. The total acquisition time of a single measure is 60 s which allows to obtain a good statistic. The experimental setup used is that described in chapter 4. The following table reports the coincidences values for each angle combination. Since laser impulse is a coherent light and therefore it has a Poisson statistic[20], the error due to the statistical fluctuation is the square root of the measure.

	α	$\alpha_\perp$	α'	$\alpha'_\perp$
β	922 ± 30	5378 ± 73	1018 ± 32	5476 ± 74
$\beta_\perp$	5261 ± 73	871 ± 30	5347 ± 73	963 ± 31
β'	4980 ± 71	1088 ± 33	1033 ± 32	5681 ± 75
$\beta'_\perp$	1047 ± 32	5169 ± 72	5492 ± 74	990 ± 31

Table 6.1: Counts regarding the test Bell inequality for polarized entangled states.

For this coincidences values, the $E(\alpha_i, \beta_i)$ becomes

$$\begin{aligned} E(\alpha, \beta) &= -0.712 \pm 0.006 \\ E(\alpha', \beta) &= -0.691 \pm 0.006 \\ E(\alpha, \beta') &= 0.652 \pm 0.007 \\ E(\alpha', \beta') &= -0.693 \pm 0.006 \end{aligned} \tag{6.7}$$

and finally we obtain

$$S = -2.75 \pm 0.01 \tag{6.8}$$

We can note that the absolute values of $E(\alpha_i, \beta_i)$ are different from each other. This suggest that the entangled state $|\Psi\rangle = \frac{1}{\sqrt{2}}\left(|HV\rangle + e^{i\pi}|VH\rangle\right)$ has a phase near π, but not equal. It can also be noted that S is less than the value expected from quantum mechanics. This is due to: the slight deviation of the phase from π and because the visibility wasn't maximum but around 97%. Even with this problem the inequality is strongly violated at $57.98\,\sigma$ like expected by quantum mechanics.

Time-bin

The time-bin measurement has been performed using the polarization measurers set in a maximum of the polarization interference. The total acquisition time of a single measure corresponds to 11s. We couldn't take a longer measurement because the Mira-HP was unstable due to the high outside temperature which didn't allow the laser source to work within the correct parameters. Only the middle peaks were used to calculate the coincidences since we are interested in the time-bin entangled photons. The experimental setup used is that described in chapter 4. The interferometers stabilization algorithm explained in section 5.3 has been used to set the measure angle. The coincidences values that we obtain performing these operations are reported in the following table.

	α	$\alpha_\perp$	α'	$\alpha'_\perp$
β	172 ± 13	915 ± 30	149 ± 12	818 ± 29
$\beta_\perp$	897 ± 30	141 ± 12	967 ± 29	187 ± 14
β'	815 ± 29	185 ± 14	164 ± 13	811 ± 28
$\beta'_\perp$	190 ± 14	877 ± 30	881 ± 30	167 ± 13

Table 6.2: Counts regarding the test Bell inequality for time-bin entangled states.

From this coincidence values we get

$$\begin{aligned} E(\alpha, \beta) &= -0.71 \pm 0.02 \\ E(\alpha', \beta) &= -0.67 \pm 0.02 \\ E(\alpha, \beta') &= 0.64 \pm 0.02 \\ E(\alpha', \beta') &= -0.67 \pm 0.02 \end{aligned} \tag{6.9}$$

from which we obtain

$$S = -2.68 \pm 0.03 \tag{6.10}$$

In this case, it can be noted that the values of $E(\alpha_i, \beta_i)$ are similar from each other considering the error. This could be due either that the error is too high to note the difference because of the limited values of the coincidences and because there isn't any phase deviation of the entangled state. Even in this good condition the value of S is less than the one expected from quantum mechanics. The main reason is that even in this case the visibility isn't maximum but around 95%. However a high violation value it's found at $20.88\,\sigma$ as expected by quantum mechanics.

6.2 "Chained" Bell Measurement

These measurements have been performed with the aim to verify whether a local realist model with long realist delays can be used to describe the physical results or not. (see section 3.3).

Like already explained, the normal Bell inequality can not answer this question so we used the so called "chained" Bell inequality that implies a generalization at more than four parameters of the classical Bell inequality. Calling A_i and B_i the angles used for measurements, the obvious generalization of $|S|$ at 6, 8, 10 parameters with the relative bond are:

$$\begin{aligned} S = |&E(A_1 B_3 | coinc.\, for\, A_1\, and\, B_3) + E(A_1 B_2 | coinc.\, for\, A_1\, and\, B_2) \\ &+ E(A_2 B_2 | coinc.\, for\, A_2\, and\, B_2) + E(A_2 B_1 | coinc.\, for\, A_2\, and\, B_1) \\ &+ E(A_3 B_1 | coinc.\, for\, A_3\, and\, B_1) - E(A_3 B_3 | coinc.\, for\, A_3\, and\, B_3)| \leq 5 \end{aligned} \tag{6.11}$$

α	β	$C(\alpha,\beta)$	$C(\alpha_\perp,\beta)$	$C(\alpha,\beta_\perp)$	$C(\alpha_\perp,\beta_\perp)$	$E(\alpha,\beta)$
0	$\frac{\pi}{6}$	1438 ± 38	119 ± 11	119 ± 11	1490 ± 39	0.850 ± 0.009
$\frac{2}{6}\pi$	$\frac{\pi}{6}$	1451 ± 38	115 ± 11	107 ± 10	1460 ± 38	0.858 ± 0.009
$\frac{2}{6}\pi$	$\frac{3}{6}\pi$	1414 ± 38	89 ± 9	144 ± 12	1456 ± 38	0.850 ± 0.009
$\frac{4}{6}\pi$	$\frac{3}{6}\pi$	1463 ± 38	75 ± 9	105 ± 10	1474 ± 38	0.885 ± 0.008
$\frac{4}{6}\pi$	$\frac{5}{6}\pi$	1460 ± 38	122 ± 11	112 ± 11	1294 ± 36	0.843 ± 0.010
0	$\frac{5}{6}\pi$	86 ± 9	1504 ± 39	1382 ± 37	103 ± 10	-0.877 ± 0.009

Table 6.3: Counts regarding the "chained" Bell inequality at 6 parameters.

$$\begin{aligned} S = |&E(A_1B_4|coinc.\,for\,A_1\,and\,B_3) + E(A_1B_3|coinc.\,for\,A_1\,and\,B_2) \\ &+E(A_2B_3|coinc.\,for\,A_2\,and\,B_2) + E(A_2B_2|coinc.\,for\,A_2\,and\,B_1) \\ &+E(A_3B_2|coinc.\,for\,A_3\,and\,B_1) + E(A_3B_1|coinc.\,for\,A_3\,and\,B_3) \\ &+E(A_4B_1|coinc.\,for\,A_3\,and\,B_1) - E(A_4B_4|coinc.\,for\,A_3\,and\,B_3)| \leq 7 \end{aligned} \tag{6.12}$$

$$\begin{aligned} S = |&E(A_1B_5|coinc.\,for\,A_1\,and\,B_3) + E(A_1B_4|coinc.\,for\,A_1\,and\,B_2) \\ &+E(A_2B_4|coinc.\,for\,A_2\,and\,B_2) + E(A_2B_3|coinc.\,for\,A_2\,and\,B_1) \\ &+E(A_3B_3|coinc.\,for\,A_3\,and\,B_1) + E(A_3B_2|coinc.\,for\,A_3\,and\,B_3) \\ &+E(A_4B_2|coinc.\,for\,A_3\,and\,B_1) + E(A_4B_1|coinc.\,for\,A_3\,and\,B_3) \\ &+E(A_5B_1|coinc.\,for\,A_3\,and\,B_1) - E(A_5B_5|coinc.\,for\,A_3\,and\,B_3)| \leq 9 \end{aligned} \tag{6.13}$$

where the condition on the angles is that the difference of b_3, a_1, b_2, a_2, b_1, a_3; b_4, a_1, b_3, a_2, b_2, a_3, b_1, a_4 ;b_5, a_1, b_4, a_2, b_3, a_3, b_2, a_4, b_1, a_5 is respectively $\pi/6$, $\pi/8$, $\pi/10$. Likewise we show in section , the error propagation for S is

$$\sigma_S = \sqrt{\sigma_{E_1}^2 + \sigma_{E_2}^2 + \ldots + \sigma_{E_{N/2}}^2} \tag{6.14}$$

where N represents the number of parameters. All the chained Bell's inequalities have been performed with the experimental setup described in chapter 4 but without using the free space channel and instead using fiber. Furthermore the interferometers stabilization algorithm has been used to set the measure angle. Since we are working with time-bin entangled state the coincidence values are calculated using only the middle peak of the entangled photons. In order to maximize the coincidences, the polarization measurers have been set in a maximum of the polarization interference.

6 Parameters "Chained" Bell Inequality

In the following table we can see the coincidences values for each combination of angle needed for the measurement regarding an acquisition time of 24s.

With these values we find that

$$S_{exp} = 5.163 \pm 0.022. \tag{6.15}$$

α	β	$C(\alpha,\beta)$	$C(\alpha_\perp,\beta)$	$C(\alpha,\beta_\perp)$	$C(\alpha_\perp,\beta_\perp)$	$E(\alpha,\beta)$
0	$\frac{\pi}{8}$	1741 ± 42	129 ± 11	119 ± 11	1791 ± 42	0.869 ± 0.008
$\frac{2}{8}\pi$	$\frac{\pi}{8}$	1803 ± 42	88 ± 9	74 ± 9	1779 ± 42	0.914 ± 0.007
$\frac{2}{8}\pi$	$\frac{3}{8}\pi$	1831 ± 43	137 ± 12	133 ± 12	1788 ± 42	0.861 ± 0.009
$\frac{4}{8}\pi$	$\frac{3}{8}\pi$	1862 ± 43	65 ± 8	57 ± 8	1789 ± 42	0.935 ± 0.006
$\frac{4}{8}\pi$	$\frac{5}{8}\pi$	1691 ± 41	150 ± 12	124 ± 11	1750 ± 42	0.853 ± 0.009
$\frac{6}{8}\pi$	$\frac{5}{8}\pi$	1899 ± 44	53 ± 7	76 ± 9	1821 ± 43	0.933 ± 0.006
$\frac{6}{8}\pi$	$\frac{7}{8}\pi$	1778 ± 42	100 ± 10	125 ± 11	1625 ± 40	0.876 ± 0.008
0	$\frac{7}{8}\pi$	75 ± 9	1815 ± 43	1718 ± 41	56 ± 7	-0.929 ± 0.006

Table 6.4: Counts regarding the "chained" Bell inequality at 10 parameters.

Knowing that the bound for the model questioned is 5 we have found a violation of the model of $7.25\,\sigma$. About the 6 parameters Bell's inequality we note that at the beginning the $E(\alpha,\beta)$ values, considering their errors, were indistinguishable from each others (the first three measures). Instead in the last ones a slight difference can be noted. This is probably caused by some thermal effect that introduces a slight phase shift on the time-bin entangled state, which it can not be compensated for by the interferometers stabilization algorithm. However this shift remains limited and can be neglected in order to find the violation. Likewise to the Bell's inequality even here we found that the S value is less than the one expected from quantum mechanics ($6\cos(\pi/6) \approx 5.196$) however it's very near to the expected one. In fact this measure has been performed with a visibility of 99.4%. This allows to find a violation with a high "contrast" with respect to the standard deviation that close the "post selection" loophole and to confirm that a local realist model with long realist delays can not describe the physical results.

8 Parameters "Chained" Bell Inequality

We report in the following table coincidences values for a "chained" bell inequality at 8 parameters with an acquisition time of 24s.

Thanks to these values we find that

$$S_{exp} = 7.169 \pm 0.020. \tag{6.16}$$

Knowing that the bound for the model questioned is 7 we have found a violation of the model of $8.25\,\sigma$. It can be note that the $E(\alpha,\beta)$ values are composed of two sets of data: one with absolute values under 0.88 and the other with absolute values grater than 0.91. This is due to a slight shift of the phase from 0 of the time-bin entangled state ($|\Psi\rangle = \frac{1}{\sqrt{2}}\left(|SS\rangle + e^{i\varphi}|LL\rangle\right)$, where φ is near but not zero). However thanks to high visibility of the entangled state ($> 97\%$) even considering this problem a violation of the chained Bell's inequality with high "contrast" with respect to the standard deviation was found. This result closes the "post selection" loophole and confirms that a local realist model with long realist delays can not describe the physical results.

α	β	$C(\alpha,\beta)$	$C(\alpha_\perp,\beta)$	$C(\alpha,\beta_\perp)$	$C(\alpha_\perp,\beta_\perp)$	$E(\alpha,\beta)$
0	$\frac{\pi}{10}$	2631 ± 51	107 ± 10	72 ± 8	2717 ± 52	0.935 ± 0.005
$\frac{2}{10}\pi$	$\frac{\pi}{10}$	2446 ± 49	81 ± 9	105 ± 10	2747 ± 52	0.931 ± 0.005
$\frac{2}{10}\pi$	$\frac{3}{10}\pi$	2545 ± 50	83 ± 9	83 ± 9	2694 ± 52	0.939 ± 0.005
$\frac{4}{10}\pi$	$\frac{3}{10}\pi$	2640 ± 51	99 ± 10	92 ± 10	2620 ± 51	0.930 ± 0.005
$\frac{4}{10}\pi$	$\frac{5}{10}\pi$	2648 ± 51	67 ± 8	74 ± 9	2783 ± 53	0.949 ± 0.004
$\frac{6}{10}\pi$	$\frac{5}{10}\pi$	2651 ± 51	144 ± 12	132 ± 11	2639 ± 51	0.901 ± 0.006
$\frac{6}{10}\pi$	$\frac{7}{10}\pi$	2667 ± 52	76 ± 9	99 ± 10	2775 ± 53	0.938 ± 0.005
$\frac{8}{10}\pi$	$\frac{7}{10}\pi$	2652 ± 51	157 ± 13	122 ± 11	2549 ± 50	0.898 ± 0.006
$\frac{8}{10}\pi$	$\frac{9}{10}\pi$	2618 ± 51	63 ± 8	43 ± 7	2647 ± 51	0.961 ± 0.004
0	$\frac{9}{10}\pi$	177 ± 13	2641 ± 51	2512 ± 50	124 ± 11	-0.890 ± 0.006

Table 6.5: Counts regarding the "chained" Bell inequality at 10 parameters.

10 Parameters "Chained" Bell Inequality

In the following table the coincidences values for a "chained" bell inequality at 10 parameters are reported with an acquisition time of 24s.

Using these values we find that

$$S_{exp} = 9.271 \pm 0.016. \tag{6.17}$$

Knowing that the bound for the model questioned is 9 we have found a violation of the model of $16.94\,\sigma$. Likewise to the 6 parameters chained Bell's inequality, even in this measurement at 10 parameters we have found at the beginning that the $E(\alpha,\beta)$ values, considering their errors, were indistinguishable from each others (first four measures). The following values instead are separated in two sets of data: one higher values and one lower values than the first ones. This, likewise to the previous chained Bell's inequality, is due to a shift of the phase of the time-bin entangled state caused by some thermal effect. However thanks to the high visibility ($> 97\%$) a violation with high "contrast" with respect to the standard deviation was found. This expected result closes the "post selection" loophole and confirms that a local realist model with long realist delays can not describe the physical results.

6.3 Quantum State Tomography

In this section we show the results about quantum state tomography of free space propagation of hyper-entangle state in polarization and time-bin DOFs. In this tomography we consider polarization and time-bin separated, obtaining two different 4x4 density matrices. All the tomography measurements have been performed with the experimental setup described in chapter 4 using the free space channel.

Polarization

In the following table we report the counts with the correspondent state regarding an acquisition time of 12s (higher time measurements could not be performed due to the high instability of the laser source caused to the high temperature of the environment). This measurement has been performed blocking the path light of the long arm of the Alice and Bob interferometers in order to avoid Time-bin interference. To calculate the coincidences all the entangled peaks have been used in order to maximize the coincidences since we are interested only to the polarization entangled state. The interferometers stabilization algorithm wasn't used during this measurement.

ν	Mode 1	Mode 2
1	$\|HH\rangle$	0
2	$\|HV\rangle$	245 ± 16
3	$\|VV\rangle$	0
4	$\|VH\rangle$	250 ± 16
5	$\|RH\rangle$	126 ± 11
6	$\|RV\rangle$	122 ± 11
7	$\|DV\rangle$	131 ± 11
8	$\|DH\rangle$	104 ± 10
9	$\|DR\rangle$	105 ± 10
10	$\|DD\rangle$	13 ± 4
11	$\|RD\rangle$	156 ± 12
12	$\|HD\rangle$	123 ± 11
13	$\|VD\rangle$	124 ± 11
14	$\|VL\rangle$	107 ± 10
15	$\|HL\rangle$	112 ± 11
16	$\|RL\rangle$	229 ± 15

Performing a Maximum Likelihood Estimates using Mathematica (see section 5.6), we obtain the density matrix

$$\hat{\rho}_{POL} = \begin{pmatrix} 0.0058 & 0.0126 - 0.0134i & -0.0302 - 0.0037i & -0.0054 + 0.0035i \\ 0.0126 + 0.0134i & 0.4885 & -0.4370 - 0.1050i & 0.0121 + 0.0023i \\ -0.0302 + 0.0037i & -0.4370 + 0.1050i & 0.4962 & -0.0029 - 0.0256i \\ -0.0054 - 0.0035i & 0.0121 - 0.0023i & -0.0029 + 0.0256i & 0.0094 \end{pmatrix} \tag{6.18}$$

Now we introduce a new important parameter, that is the Fidelity. Like the name suggests, it characterizes how much the recovered matrix is similar to the theoretical ones. It's defined as

$$\mathcal{F} = Tr(\hat{\rho}\hat{\rho}_{Theo}) \tag{6.19}$$

where $\hat{\rho}_{Theo}$ represents the density matrix for the entangled state (see formula 5.42).

Furthermore we remember the importance of the Purity (1.25) that expresses how close the matrix recovery is to a pure state.

Thus the values of these two parameters are

$$\begin{aligned} \mathcal{F} &= 92.94\% \\ \mathcal{P} &= 89.32\% \end{aligned} \tag{6.20}$$

These results confirm that what we have detected was a polarization entangled state. Observing the figure 6.2 we can note that the imaginary values of $|VH\rangle\langle HV|$ and $|HV\rangle\langle VH|$ are a little high. This is caused by the presence of an offset in respect of the correct position of one or more wave plates. This explain also the reason of the not high values of the fidelity and purity.

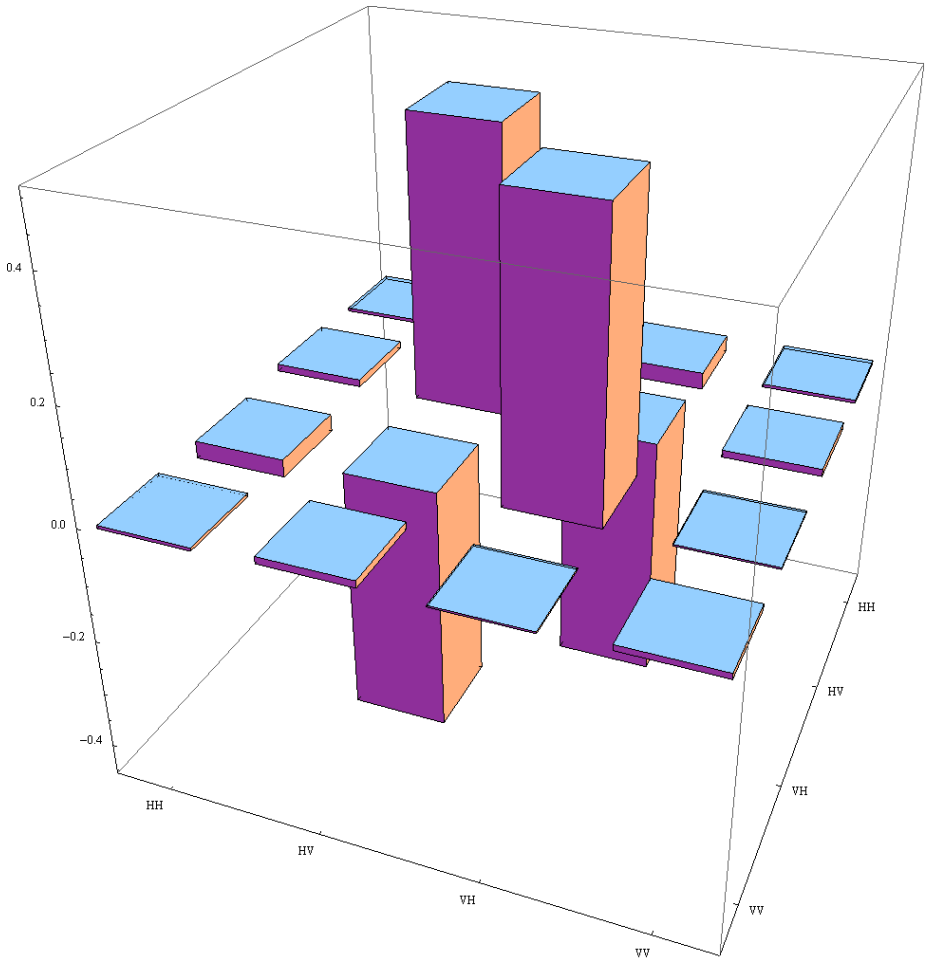

Figure 6.1: Real values of the polarization density matrix $\hat{\rho}_{POL}$

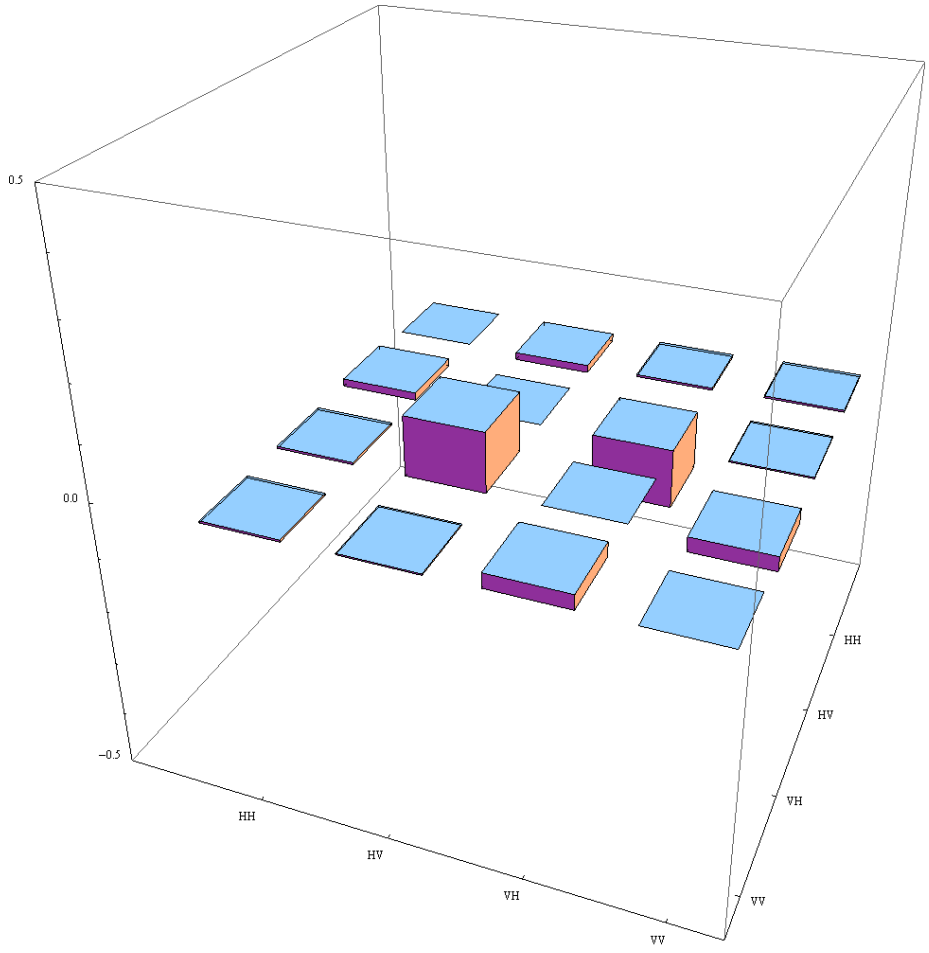

Figure 6.2: Imaginary values of the polarization density matrix $\hat{\rho}_{POL}$. It can be noted that there are non zero values for the states $|HV\rangle\langle VH|$ and $|VH\rangle\langle HV|$. This could be due to a slight offset of the zero axis on the $\lambda/2$ and $\lambda/4$ plates.

Time-bin

In the following table we report the counts with the correspondent state regarding an acquisition time of 24s (higher time measurements could not be performed due to the high instability of the laser source caused to the high temperature of the environment). This measurement has been performed using the interferometers stabilization algorithm and blocking, when needed, the light path of the arms of the interferometers in order to project the entangled state to the several states needed to execute the tomography. In order to maximize the coincidences the polarization measurer has been set in a maximum of the polarization interference. Since we are interested in time-bin entangled state,

to calculate the coincidences we used only the middle peak.

ν	Mode 1	Mode 2
1	$\|Short\, Short\rangle$	535 ± 23
2	$\|Short\, Long\rangle$	2 ± 1
3	$\|Long\, Long\rangle$	486 ± 22
4	$\|Long\, Short\rangle$	16 ± 4
5	$\|R\, Short\rangle$	272 ± 16
6	$\|R\, Long\rangle$	233 ± 15
7	$\|D\, Long\rangle$	204 ± 14
8	$\|D\, Short\rangle$	277 ± 17
9	$\|DR\rangle$	256 ± 16
10	$\|DD\rangle$	505 ± 22
11	$\|RD\rangle$	226 ± 15
12	$\|ShortD\rangle$	304 ± 17
13	$\|Long\, D\rangle$	236 ± 15
14	$\|Long\, L\rangle$	193 ± 14
15	$\|ShortL\rangle$	255 ± 16
16	$\|RL\rangle$	524 ± 23

Regarding the time-bin entangled state, the correspondent density matrix can be found in formula 5.44. Performing a Maximum Likelihood Estimates we recover the density matrix

$$\hat{\rho}_{Time-bin} = \begin{pmatrix} 0.5252 & 0.0006 - 0.0062i & -0009 + 0.0126i & 0.4762 + 0.0350i \\ 0.0006 + 0.0062i & 0.0090 & -0.0058 - 0.0070i & -0.0107 + 0.0077i \\ -0.0088 - 0.0126i & -0.0058 + 0.0070i & 0.0150 & -0.0041 - 0.0252i \\ 0.4762 - 0.0350i & -0.0107 - 0.0077i & -0.0041 + 0.0252i & 0.4508 \end{pmatrix} \tag{6.21}$$

In the end we report the purity and the fidelity of the recovered matrix that insures that we have recorded the right states.

$$\begin{aligned} \mathcal{F} &= 96.42\% \\ \mathcal{P} &= 93.78\% \end{aligned} \tag{6.22}$$

The values of purity and fidelity are high enough to affirm with high probability that what we have measured is $|\Psi\rangle = \frac{1}{\sqrt{2}}(|SS\rangle - |LL\rangle)$. This can be also deduced observing the figures 6.3 and 6.4 where we see a density matrix very similar to the theoretical one (see formula 5.44).

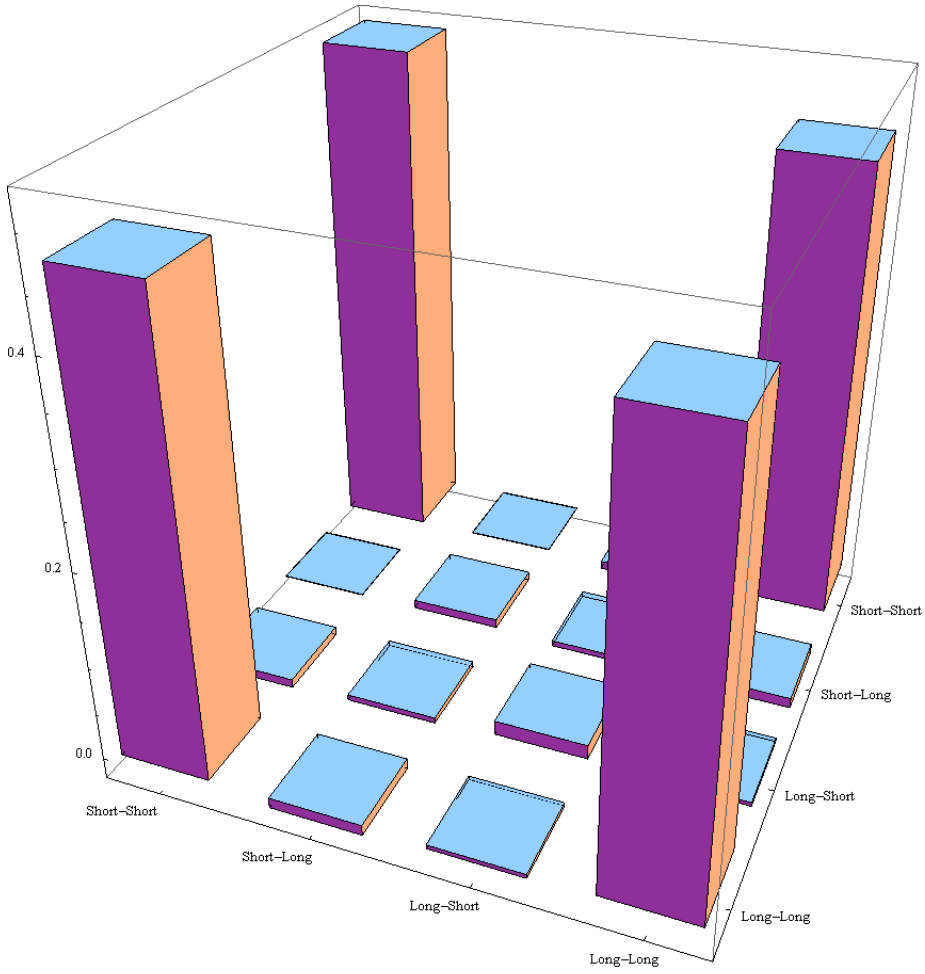

Figure 6.3: Real values of the time-bin density matrix $\hat{\rho}_{Time-bin}$

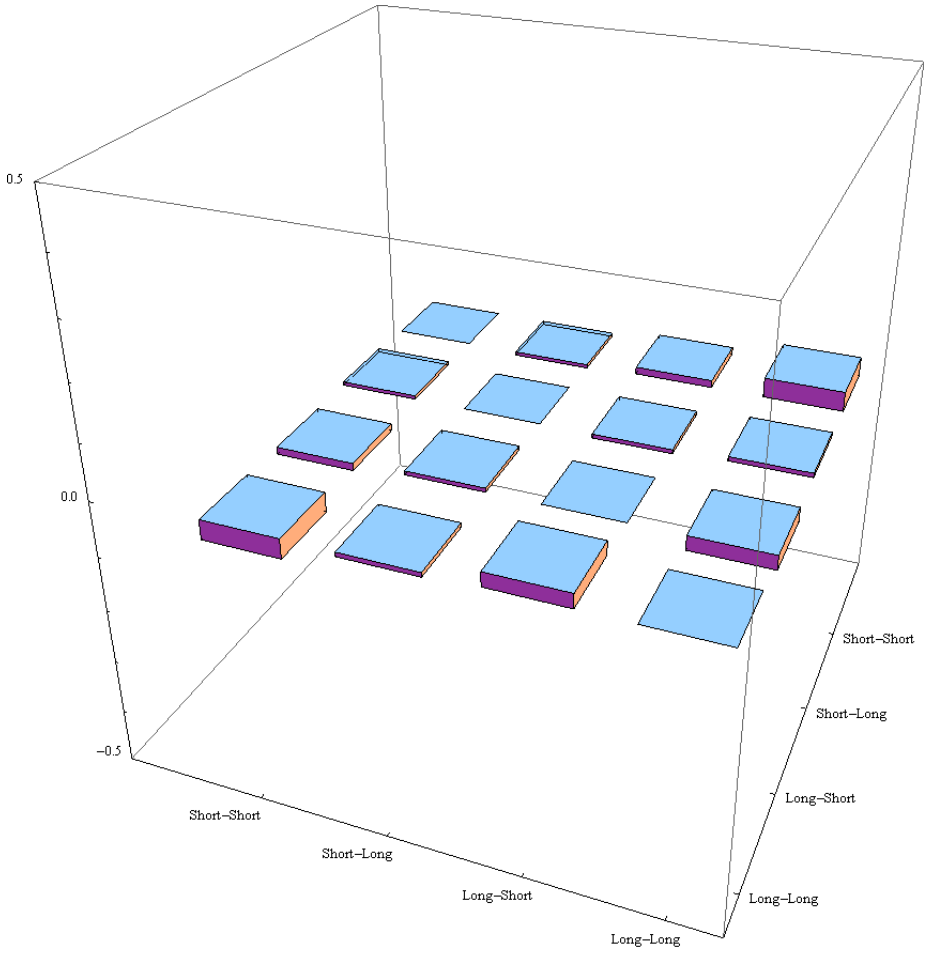

Figure 6.4: Imaginary values of the time-bin density matrix $\hat{\rho}_{Time-bin}$.

6.4 Results

The results that we achieve with these experiments are:

- A violation with high "contrast" of the "chained" Bell inequality ($7.25\,\sigma$, $8.25\,\sigma$, $16.94\,\sigma$ respectively for a "chained" bell in equality at 6, 8, 10 parameters) which proves that a realist model with long realist delays does not describe the physical results as expected by quantum mechanics

- A strong violation of the Bell's inequality ($57.98\,\sigma$, $20.88\,\sigma$ respectively for polarization e time-bin entangled photons) when we send hyperentangled photons using a free-space channel. This demonstrated that even when we send the hyperentangled photons using a free-space channel, Alice and Bob

found that the received photons are entangled in time-bin and polarization degrees of freedom

- A high fidelity and purity of the density matrix calculated by a maximum likelihood estimates compared to the ones of the prepared state (92.94%, 96.42% of fidelity and 89.32%, 93.78% of purity respectively for polarization e time-bin entangled photons). This proves that the polarization and time bin entangled states prepared are preserved when we send the photons using a free-space channel.

All these results confirm the initial goals (to demonstrate that a local realist model with long realist delays can not describe the physical results and to successfully perform an hyperentangled communication in free space using photons as a means) have been achieved.

Conclusion

With this thesis, we perform an experiment proving that local realist model with long realist delays cannot be used to describe the physical results. Furthermore we have successfully sent hyperentangled quantum states using a free space link. The main steps that help me to get this results were:

- Accustom with the production of time-bin entangled states and polarization entangled states in order to create a hyperentangled states in polarization and time-bin degrees of freedom.
- Develop a system to stabilize the interferometer in order to correct the instability introduced by the thermal expansion and the wavelength drift of the laser source.
- Enhance the previous synchronization system in order to adapt to the stabilization system by developing a dynamic library that takes into account the number of triggers registered by the beginning of the synchronization.
- Perform measurements of "chained" Bell inequality at high visibility to prove that local realist model with long realist delays cannot be used to describe the physical results.
- After having established a free space channel to send Bob qubits, perform measurements of Bell inequality to prove that the states remain entangled after the free-space propagation.
- Perform quantum states tomography in time-bin and polarization degrees of freedom to prove that hyper-entangled states maintain themselves unchanged during free space propagation.

The results shown in the last chapter, prove that we was able to demonstrate that local realist model with long realist delays cannot be used to describe the physical results. Furthermore the quantum states tomography measurements prove that we successfully sent entangled states in time-bin and polarization using a free space channel of about 3 meters. A next step could be to perform a hyperentangled tomography[1] that requires different kind of tomography techniques and then to increase the distance of the free space channel in order to

[1] the density matrix is a 16×16 matrix, that using Likelihood Estimates require 256 measurements

perform free space quantum communication at long distance. In particular free space quantum communication at long distance could be very important as a first step:

- to perform super-dense coding in free space at long distance that could be used to increase the density of the information sent,
- to perform quantum teleportation in more degrees of freedom that could be used to send more than one quantum states with a single particle with higher efficiency using a classical channel.

Bibliography

[1] W. K. Wootters and W. H. Zurek, "A single quantum cannot be cloned," *Nature*, vol. 299, pp. 802 – 803, 1982.

[2] B. Korzh, C. C. W. Lim, R. Houlmann, N. Gisin, M. J. Li, D. Nolan, B. Sanguinetti, R. Thew, and H. Zbinden, "Provably secure and practical quantum key distribution over 307 km of optical fibre," *Nature Photonics*, vol. 9, pp. 163–168, 2015.

[3] T. Schmitt-Manderbach, H. Weier, M. Fürst, R. Ursin, F. Tiefenbacher, T. Scheidl, J. Perdigues, Z. Sodnik, C. Kurtsiefer, J. G. Rarity, A. Zeilinger, and H. Weinfurter, "Experimental demonstration of free-space decoy-state quantum key distribution over 144 km," *Phys. Rev. Lett. 98, 010504*, vol. 98, 2007.

[4] C. Bennett and G. Brassard, "Quantum cryptography: Public key distribution and coin tossing," in *Proc. of the IEEE Int. Conf. on Computers, Systems & Signal Processing*, vol. 175, pp. 175–179, 1984.

[5] G. Brassard and C. H. Bennett, "Quantum cryptography without Bell's theorem," *Phys. Rev. Lett.*, vol. 68, 1992.

[6] A. K. Ekert, "Quantum cryptography based on Bell's theorem," *Phys.Rev. Lett*, vol. 67, 1991.

[7] G. Bennett Brassard, C. Crepeau, R. Jozs, and A. Peres, "Teleporting an unknown quantum state via dual classical and Einstein-Podolsky-Rosen channels," *Phys. Rev. Lett.*, vol. 70, pp. 1895–1899, 1993.

[8] D. Bouwmeester, J. W. Pan, K. Mattle, M. Eibl, H. Weinfurter, and A. Zeilinger, "Experimental quantum teleportation," *Nature*, vol. 390, pp. 575–579, 1997.

[9] P. et al., "Experimental entanglement swapping: Entangling photons that never interacted," *Phys. Rev. Lett.*, vol. 80, pp. 3891–3894, 1998.

[10] J. T. Barreiro, T. Wei, and P. Kwiat, "Beating the channel capacity limit for linear photonic superdense coding," *Nature Physics*, 2008.

[11] K. Mattle, H. Weinfurter, P. G. Kwiat, and A. Zeilinger, "Dense coding in experimental quantum communication," *Phys. Rev. Lett.*, vol. 76, pp. 4656–4659, Jun 1996.

[12] H. R. Morton, "Transverse correlation in optical spontaneous parametric downconversion," *Phys. Rev. A*, pp. 5349–5360, 1996.

[13] J. S. Bell, "On the Einstein-Podolsky-Rosen paradox," *Physics (N. Y.)*, vol. 1, pp. 195–200, 1964.

[14] A. Aspect, J. Dalibard, and G. Roger, "Experimental test of Bell's inequalities using time- varying analyzers," *Phys. Rev. Lett.*, vol. 49, pp. 1804–1807, 1982.

[15] P. Pearle, "Hidden-variable example based upon data rejection," *Phys. Rev. D*, vol. 2, pp. 1418–1425, 1970.

[16] M. A. Rowe, D. Kielpinski, V. Meyer, C. A. Sackett, W. M. Itano, C. Monroe, and D. J. Wineland, "Experimental violation of a Bell's inequality with efficient detection," *Nature*, vol. 409, pp. 791–794, 2001.

[17] B. Hensen, H. Bernien, A. Dréau, A. Reiserer, N. Kalb, M. Blok, J. Ruitenberg, R. Vermeulen, R. Schouten, C. Abellán, W. Amaya, V. Pruneri, M. Mitchell, M. Markham, D. Twitchen, D. Elkouss, S. Wehner, T. Taminiau, and R. Hanson, "Experimental loophole-free violation of a Bell inequality using entangled electron spins separated by 1.3 km," *arXiv:1508.05949*, 2015.

[18] S. Aerts, P. Kwiat, J.-A. Larsson, and M. Z˙ukowski, "Two-photon Franson-type experiments and local realism," *Phys. Rev. Lett.*, vol. 83, pp. 2872–2875, Oct 1999.

[19] J. Jonathan and L. Jan-Åke, "Energy-time entanglement, Elements of Reality, and Local Realism," *arXiv:1103.6131*, 2011.

[20] B. E. A. Saleh and M. C. Teich, *Fundamentals of Photonics*. John Wiley & Sons, 2007.

[21] l. F. V. James Danie, G. Kwiat Paul, J. Munro William, and G. White Andrew, "Measurement of qubits," *Phys. Rev. A*, 2001.